DRAFT VERSION MARCH 20, 2024
Preprint typeset using LaTeX style emulateapj v. 04/03/99

arXiv:astro-ph/0401087v2 19 Feb 2004

QUASAR FEEDBACK: THE MISSING LINK IN STRUCTURE FORMATION

EVAN SCANNAPIECO[1] & S. PENG OH[2]

Draft version March 20, 2024

ABSTRACT

We consider the impact of quasar outflows on structure formation. Such outflows are potentially more important than galactic winds, which appear insufficient to produce the level of preheating inferred from X-ray observations of galaxy clusters. At late times, energetic material from the densest objects in the centers of galaxies makes its way into the intergalactic medium (IGM), impacting structures on many scales, much as supernovae impact structures on many scales within the interstellar medium. Using a simple analytical model for the distribution of quasars with redshift, coupled with a one-dimensional Sedov-Taylor model for outflows, we are able to make robust statements about these interactions. As large regions of the IGM are heated above a critical entropy of $S_{\rm crit}$ 100 keV cm^2, cooling become impossible within them, regardless of changes in density. On quasar scales, this has the effect of inhibiting further formation, resulting in the observed fall-off in their number densities below z 2. On galaxy scales, quasar feedback fixes the turn-over scale in the galaxy luminosity function ($L^?$) as the nonlinear scale at the redshift of strong feedback. The galaxy luminosity function then remains largely fixed after this epoch, consistent with recent observations and in contrast to the strong evolution predicted in more standard galaxy-formation models. Finally, strong quasar feedback explains why the intracluster medium is observed to have been pre-heated to entropy levels *just above* $S_{\rm crit}$; the minimum excess that would not have been erased by cooling. The presence of such outflows is completely consistent with the observed properties of the Lyman-forest at z 2, but is expected to have a substantial and detectable impact on Compton distortions observed in the microwave background and the multiphase properties of the "warm-hot" ($z = 0$) circumgalactic medium.

Subject headings: quasars: general – galaxies: evolution – intergalactic medium – large-scale structure of the universe – cosmology: theory

1. INTRODUCTION

Non-gravitational heating is known to have played a central role in the formation of galaxy clusters. This is most clearly illustrated by the observed discrepany in the X-ray Luminosity Temperature ($L_X - T$) relationship of the diffuse intracluster medium (ICM). If non-gravitational heating was unimportant, the gas density distribution would be self-similar, resulting in $L_X \propto T^2$ (Kaiser 1986), but instead the observed slope steepens considerably for low-temperature clusters (*e.g.* David et al. 1993; Arnaud & Evrard 1999; Helsdon & Ponman 2000). Non-gravitational heating also manifests itself in the anomalous hot gas fractions observed in clusters (*e.g.* Muanwong et al. 2002; Tornatore et al. 2003), as well as the low overall level of the X-ray background (Pen 1999). While the origin of this heating remains unknown, a wide variety of arguments point to the importance of active galactic nuclei, and in particular the luminous quasars. Although high-redshift starburst galaxies are observed to host massive supernova-driven outflows (*e.g.* Pettini et al. 2001), it is unlikely that they are able to generate the 1 keV of energy per gas particle required to account for cluster preheating (Cavaliere, Menci, & Tozzi 1998; Balogh, Babul & Patton 1999; Kratsov & Yepes 2000; Wu, Fabian, & Nulsen 2000; Bialek, Evrard & Mohr 2001; Borgani et al. 2001; Brighenti & Mathews 2001; Tozzi, Scharf, & Norman 2001; Babul et al 2002). In fact, this level of heating is so high that it greatly exceeds the energy available from the Type-II supernovae resulting from metal-enriched stars, as well as the additional energy input from pair-production supernovae from a possible generation of massive primordial stars (*e.g.* Scannapieco, Schneider, & Ferrara 2003). Quasars, on the other hand, represent a vast reservoir of energy that is largely untapped in current theoretical modeling.

Radiation from quasars should not be significantly coupled to the surrounding gas, except perhaps in the innermost cooling flow regions of the ICM where Compton heating or cooling could be important (Ciotti & Ostriker 1997, 2001). Nevertheless, the overall bolometric luminosities of quasars are far above the levels necessary to effectively preheat the intracluster medium (*e.g.* Inoue & Sasaki 2001; Nath & Roychowdhury 2002). Furthermore, a large fraction of quasars are observed to host massive outflows of material, with energies comparable to their observed luminosities. Thus the light observed to be emanating from quasars at intermediate redshifts, while not directly causing gas heating, is likely to be strongly correlated with outflows that provide a substantial source of non-gravitational energy.

Like their high-redshift counterparts, these outflows would have consequences beyond their impact on the intergalactic gas. Detailed studies of high-redshift dwarfs indicate that starburst-driven shells are able to strip gas out of nearby overdense regions that would have otherwise later formed stars. This gas is ejected into space, leaving behind empty "dark halos" of non-baryonic matter (Scannapieco, Ferrara, & Broadhurst 2000). As it is much easier to strip gas from small objects, such winds naturally exert a feedback effect on neighboring dwarf galaxies (Scannapieco, Ferrara, & Madau 2002), causing a tremendous decrease in their numbers and slowing the formation of further outflows.

The high entropy of preheated gas will also strongly affect

[1]Kavli Institute for Theoretical Physics, Kohn Hall, UC Santa Barbara, Santa Barbara, CA 93106
[2]Department of Physics, UC Santa Barbara, Santa Barbara, CA 93106

galaxy formation, as any level of entropy that can perturb gas density profiles in clusters will obviously have a major impact on the much shallower potential wells of galaxies. A moderate increase in entropy has been seen to reduce angular momentum loss during collapse in numerical simulations, (Mo & Mao 2002; van den Bosch et al. 2003), and may explain the reduced X-ray luminosities of late-type galaxies (Mo & Mao 2002). Further increases in entropy are able to cut-off the supply of cold gas available for galaxy formation, resulting in strong negative feedback, which may be important in determining galaxy morphology (Oh & Benson 2003), and which has direct implications for clusters.

The entropy to which clusters have been preheated is not arbitrary, but rather corresponds approximately to the threshold value for cooling within the age of the universe (Voit & Bryan 2001). Indeed, for $S > S_{\rm crit}$ 100 keV cm^2, gas can never cool within a Hubble time regardless of the density to which it is compressed, and is therefore permanently unavailable for galaxy formation (Oh & Benson 2003). Thus if non-gravitational heating in clusters had raised the gas to a somewhat lower adiabat, this energy would have been quickly radiated away, and local X-ray observations would have left us none the wiser as to its presence. Yet, if clusters had been heated much *above* $S_{\rm crit}$, such observations would have easily detected this excess. While this coincidence can only result from fine-tuning in a model that accounts only for gas heating, it is an unavoidable feature of a model that accounts for its *feedback* on the process of galaxy formation itself. As quasar outflows heat the gas around them, they shut off gas cooling, both in the intracluster medium and in the gas that is accreting into smaller objects that would have otherwise formed into galaxies. In this case, the supply of cold gas available for star formation and quasar fueling is determined as a result of a strong feedback equilibrium reached between radiative cooling and quasar heating.

It is intriguing that the redshifts at which the cores of groups and clusters were assembled (z 2 – 3) also correspond to the peak of quasar activity. Oh & Benson (2003) explored the effects of global preheating at z 2 – 3 on star-formation, cutting off the supply of cold gas, but did not consider the spatial dependence of entropy injection. In fact, more highly biased regions should be heated to high entropy at earlier epochs, implying that star-formation is self-limiting in the highest density peaks. A similar self-limiting mechanism may also operate in high-redshift star formation ($z > 10$), when the residual entropy from early reionization prevents star formation in low mass halos (Oh & Haiman 2003). However, early preheating due to galactic winds at high redshift z 10 would have little effect on the *present-day* galaxy population, since the residual entropy of the IGM heated at high-redshift is too low (Benson & Madau 2003).

While several groups have recently studied the relationship between the formation history of galaxies and the cosmological evolution of quasars, none have accounted for the global impact of quasars on the IGM and its consequences for future galaxy formation. Kauffmann & Haehnelt (2000) incorporated a simple scheme for the growth of supermassive black holes into a semi-analytic model of galaxy formation, reproducing the observed luminosity function of quasars in the context of major mergers. Ciotti & Van Albada (2001) used the observed relationship between the masses of supermassive black holes and the velocity dispersion of their hosts to study the possibility of substantial dissipationless merging in the formation of elliptical galaxies. Quasar formation regulated by local feedback was studied by Wyithe & Loeb (2003; hereafter WL03), as will be discussed in more detail below. Di Matteo et al. (2003) studied the metallicity evolution of quasar host galaxies, finding metallicity gradients and trends consistent with observations. Haiman, Ciotti, & Ostriker (2003) studied how the duty cycle of quasar activity can be constrained from the optical quasar luminosity function and the masses of host galaxies. Finally, and perhaps most directly related, Granato et al. (2003) studied the co-evolution of quasars and spheroidal galaxies, and the impact of quasar-driven winds on the gas *within* such galaxies.

In this paper we adopt a more global view, in an attempt to understand the features that emerge when quasar feedback is accounted for in current scenarios of structure formation. Using a simple analytical model for the distribution of quasars with redshift, coupled with a one-dimensional Sedov-Taylor model for the outflows associated with these sources, we analyze the impact of quasars on galaxy formation, the structure of the intergalactic medium, and the further formation of quasars themselves. Despite the relative simplicity of our approach, we are able to make robust statements as to the general features of strong feedback models that differ from more standard scenarios, as well as indicate which observational constraints can be used to most easily discriminate between the two.

Throughout this paper we restrict our attention to a Cold Dark Matter (CDM) cosmological model with parameters h = 0.7, $_m$ = 0.3, = 0.7, $_b$ = 0.045, $_8$ = 0.87, and n = 1, where h is the Hubble constant in units of 100 km s^{-1} Mpc^{-1}, $_m$, , and $_b$ are the total matter, vacuum, and baryonic densities in units of the critical density, $^2_8$ is the variance of linear fluctuations on the $8h^{-1}$Mpc scale, and n is the "tilt" of the primordial power spectrum. These choices are motivated mainly by measurements of the cosmic microwave background, the number abundance of galaxy clusters, and high-redshift supernova distance estimates (*e.g.* Spergel et al. 2003; Eke et al. 1996; Perlmutter et al. 1999). Finally, we make use of the Eisenstein and Hu (1999) fit to the transfer function in computing the matter power-spectrum.

The structure of this work is as follows. In §2 we describe a simple model of the quasar luminosity function (WL03), which relates the formation rate of quasars to the merger rate of collapsed dark-mater halos. In §3 we consider the scales of quasar outflows, and in §4 we develop a model for the spatial distribution of the resulting high-entropy material and its feedback on structure formation. In §5 we consider the impact of this feedback on the formation of quasars and galaxies, contrast it with higher-redshift feedback effects, and examine the impact of quasar outflows on the observed properties of the IGM at high and low redshifts. A discussion is given in §6.

2. QUASAR POPULATION

The first step in studying the impact of quasars on structure formation is to model their overall distribution. As discussed by Yu & Lu (2003), any such model is limited by two major constraints. The first of these is the observed number density of quasars, which has been well-measured out to redshifts $<$ 6. Secondly, as quasars are believed to be powered by supermassive black holes (*e.g.* Blandford & Znajek 1977), such models must reproduce the measured black hole mass - bulge velocity dispersion ($M_{\rm bh} - _c$) relation.

While a wide variety of models of quasar formation have been suggested within the CDM paradigm (Efstathiou & Rees

1988; Haehnelt & Rees 1993; Kauffmann & Haehnelt 2000; Nulsen & Fabian 2000; Monaco, Salucci, & Danese 2000; Haiman & Loeb 2001; Wyithe & Loeb 2002; Menci et al. 2003; Bromley, Somerville, & Fabian 2003), these can be roughly divided into two types. In early studies, quasar formation rates were tied to the formation rates of dark matter halos, as given by the rate of change in the Press & Schechter (1974, hereafter PS) mass function of dark mater halos. As both observational constraints and theoretical tools improved, such models were widely superseded by approaches that tied quasar formation to mergers between dark mater halos. Theoretically, this had the advantage of eliminating poorly defined "halo formation times," as well avoiding corrections due to the fact that the derivative of the PS mass function counts both the formation of objects of a given mass as well as their "destruction" by merging into larger objects. Observationally, on the other hand, there is considerable evidence to support the idea that quasars are formed in mergers (*e.g.* Osterbrok 1993). A large fraction of quasar hosts display a disturbed morphology (*e.g.* Smith et al. 1986), have nearby companions (*e.g.* Vader et al. 1987), or even posses features that can be interpreted as tidal tails (Stockton & Ridgway 1991). Furthermore, the existence of the tight $M_{\rm bh} - {}_c$ correlation suggests that quasar formation is closely related to bulge formation, which itself is thought to be triggered by mergers (*e.g.* Barnes & Hernquist 1992). Finally, we note that even the merger prescription is not enough to model the low-redshift quasar population, which exhibits a strong decrease at $z < 2$. This is traditionally interpreted as due to the ever-increasing gas cooling times within larger halos (*e.g.* Rees & Ostriker 1977), but also arises in a model of strong quasar feedback, as we shall see below.

As the focus of our investigation is not the detailed modeling of the processes of quasar formation, but rather the global feedback of this population on structure formation as a whole, we do not attempt a survey of these quasar models. Rather we make use of the simple and elegant model developed in WL03 and Wyithe & Loeb (2002), which satisfies both types of constraints in the context of major mergers. Furthermore, as the model is constructed only to reproduce the distribution of $z > 2$ quasars, it contains no prescription for gas cooling and accretion at low redshifts that might otherwise obscure our results.

Instead, the authors simply assume that following a merger, a black hole shines at its Eddington luminosity (as observed by *e.g.* Willott, McLure, & Jarvis 2003), and returns a fraction of this energy to the galactic gas, eventually disrupting its own fuel source. In this case a quasar shines for the dynamical time of the cold gas surrounding the black hole, which is usually located in a disk with a characteristic radius ($= \sqrt{2}$)$r_{\rm vir}$ $0.035\kappa_{\rm vir}$ (Mo, Mao, & White 1998). The corresponding dynamical time is then (*e.g.* Barkana & Loeb 2001)

$$t_{\rm dyn} \quad 0.035\kappa_{\rm vir}/v_{\rm c} \quad 5 \quad 10^7{\rm yr}\,(1+z)^{-3/2}; \qquad (1)$$

where 0.05 is the spin parameter, $\kappa_{\rm vir}$ is the virial radius, and $v_{\rm c}$ is the circular velocity of the galactic halo, which can be written as

$$v_{\rm c} = 140\,{\rm km\,s^{-1}}\,M_{12}^{1/3}\,(1+z)^{1/2}; \qquad (2)$$

where M_{12} $\frac{M_{\rm halo}}{10^{12}M}$. Note that the timescale given by eq. (1) is comparable to the *e*-folding time of the black hole mass or Salpeter time t_S 2.7 $10^7(\ _{\rm rad}/0.06)$yr, where $_{\rm rad}$ is the radiative efficiency.

Furthermore, this "self-regulation" condition amounts essentially to assuming that the total energy output from a quasar is proportional to the depth of the potential well of the halo in which it is contained, implying $M_{\rm bh} \propto v_{\rm c}^5$. Note however that this index is slightly larger than the 4-4.5 inferred from the local $M_{\rm bh} - {}_c$ relation (Merritt & Ferrarese 2001; Tremaine et al. 2002), the difference having its origin in the observation that the $v_{\rm c} - {}_c$ relation is shallower than linear (Ferrarese 2002). In this model the $M_{\rm bh} - v_{\rm c}$ relation is independent of redshift as observed by Sheilds et al. (2003), with

$$M_{\rm bh} = 1.4 \quad 10^8 M \quad F \quad \left(\frac{v_{\rm c}}{300\,{\rm km\,s^{-1}}}\right)^5 : \qquad (3)$$

Combining this relation with eq. (2) gives

$$M_{\rm bh}(M_{\rm halo};z) \quad {}_{\rm bh}(M_{\rm halo};z)M_{\rm halo}; \qquad (4)$$

where ${}_{\rm bh}(M_{\rm halo};z)$ ${}_{\rm bh,0}M_{12}^{\frac{2}{3}}(1+z)^{\frac{5}{2}}$; and ${}_{\rm bh,0}$ 3.2 10^6F: The only adjustable parameter in this model is F, which, in our notation, was taken to be 0.6 in WL03, and is taken to be 1.0 in our fiducial modeling below. Observations (*e.g.* Ferrarase 2002) suggest that $M_{\rm bh} = M$ $(1.66$ $0.32)$ 10^8 ${}_c/(200\,{\rm km\,s^{-1}})^{4.58\ 0.52}$ with $\log_{10}(v_c/300)$ = $(0.84$ $0.09)\log_{10}({}_c/200{\rm km/s}) + (0.0$ $0.19)$, which would allow for models with F values between 0.15 and 7.0 to fall within 1 experimental errors, due primarily to the uncertainty in the relation between v_c and ${}_c$.

2.1. *Optical Quasar Luminosity Function*

Having developed a model for quasar formation during mergers, we are now able to construct a luminosity function, $(z;L_B)$; which measures the comoving number density of quasars per unit B-band luminosity (L_B). Taking the observed relation of $L_{\rm bol} = 10.4L_B$ (Elvis 1994) means that $M_{\rm bh} = L_{{\rm Edd},B}/(5.73$ 10^3L $M^{-1})$; and we can invert eq. (4) to compute $M_{\rm halo}$ as a function L_B, relating $(z;M)$ to the merger rate as

$$(z;L_B) = \frac{3}{5\ {\rm bh}}\frac{t_{\rm dyn}(z)}{5.73 \quad 10^3L \ M^{-1}}\int_{0.25M_{\rm halo}}^{0.5M_{\rm halo}} d\ M_{\rm halo} \qquad (5)$$
$$\frac{dn}{dM^0}(z;M^0)\frac{d^2N_{\rm merge}}{d\ M_{\rm halo}dt}(z;\ M_{\rm halo};z;M_{\rm halo});$$

where M^0 $M_{\rm halo} - M_{\rm halo}$:Here the comoving density of halos with mass M is given by the usual PS prescription

$$\frac{dn}{dM}(z;M) = \frac{}{M}\frac{d\ ^2}{dM}(M)\ f[\ (z);\ ^2(M)]; \qquad (6)$$

where is the mean matter density, (z) $1.69D^{-1}(z)$ is the "collapse threshold" at a redshift z with $D(z)$ the linear growth factor, $^2(M)$ is the the variance of linear fluctuation within spheres containing a given mass M, and

$$f(\ ;\ ^2)d\ ^2 \quad \frac{}{\sqrt{2\ ^3}}\exp\ -\frac{^2}{2\ ^2}\ d\ ^2; \qquad (7)$$

is the mass fraction contained in halos with masses associated with variances in the range from ^{2} to $^2 + d\ ^2$. Finally

$$\frac{d^2N_{\rm merge}}{dM_p\,dt}(z_p;M_p;z_f;M_f) = \frac{d\ (z_f)}{dt(z_f)}\frac{@}{@\ _f}f_2 \quad {}_p;\ ^2(M_p);\ {}_f;\ ^2(M_f)\ ; \qquad (8)$$

is the rate of mergers of halos with masses between M_p and $M_p + dM_p$ and formation redshifts z_p into halos of mass M_f at a merger redshift z_f and

$$f_2(\ _p;\ ^2_p;\ _f;\ ^2_f) \quad \frac{f(\ _p - \ _f;\ ^2_p - \ ^2_f) f(\ _f;\ ^2_f)}{f(\ _p;\ ^2_p)}; \qquad (9)$$

is the conditional probability that an object with a mass M_p at a redshift z_p will be found in an object with a mass M_f at z_f (Lacey & Cole 1993).

The resulting luminosity functions are shown in Figure 1. Again we note that the WL03 model is constructed to match the quasar distribution at high redshifts, and thus assumes that all the gas within a galactic halo cools on a time much shorter than the Hubble time. This is the primary cause of the overestimate of at the lower redshifts, as eq. (6) includes an additional contribution from massive halos, which form into groups and clusters rather than individual galaxies.

3. QUASAR OUTFLOWS

In order to relate $(z; L_B)$ to the overall level of kinetic feedback, we must adopt a simple model for the formation and propagation of quasar outflows. Here two major types of objects contribute. In radio-loud (RL) quasars, the outflow takes the form of a collimated jet, which deposits particles into a cocoon that expands into the surrounding medium. These jets, which are found in 10% of all quasars, are observed to have overall kinetic luminosities (L_k) that are correlated with the bolometric luminosity of the quasars, with $0.05 < L_k/L_{bol} < 1.0$ (Willott et al. 1999). The major radio-quiet (RQ) sources, on the other hand, are broad absorption line (BAL) quasars, whose optical absorption troughs are thought to correspond to outflowing clouds with velocities up to $0.1c$. Similar velocities are also observed in outflowing material detected at X-ray wavelengths (*e.g.* Pounds et al. 2003). Although these make up approximately 10% of the observed population of quasars, it is believed that all quasars host these outflows, with a 10% covering factor (*e.g.* Weymann 1997). Again observational and theoretical arguments suggest that the impact of these clouds on the surrounding medium can be parameterized with overall kinetic luminosities correlated with the bolometric luminosities with $0.1 < L_k/L_{bol} < 10$ (Furlanetto & Loeb 2001; Nath & Roychowdhury 2002).

Do quasars that host outflows differ widely in their properties from the general quasar population? In the radio-loud case, this relation is a subject of debate. A number of earlier studies claimed that, with substantial overlap, RL quasars tended to be found in Abell 0/1 clusters, while RQ quasars generally inhabit less-dense regions (*e.g.* Yee & Green 1984; Ellingson 1991). More recent Hubble Space Telescope studies, however, have shown that to some degree this is a selection effect, with a RQ population being found in clusters (*e.g.* Bachall et al. 1997), perhaps in the same relative proportions as RL quasars (McLure & Dunlop 2001).

In the BAL case, on the other hand, the primary issue is not if the spatial distribution of objects is different from the general quasar population, but rather whether the presence of broad absorption lines represents a stage in the life cycle of quasars (*e.g.* Briggs et al. 1984), or is simply a geometric effect (*e.g.* Weymann et al. 1991). In this case the geometric interpretation is favored by the similarity between the optical continuum and line emission of BAL and non-BAL quasars (Boroson & Meyers 1992), as well as by the fact that the sub-millimeter emission of quasar host galaxies is not related to the presence of broad absorption lines (Willott et al. 2003).

Finally there is the issue of outflow structure, which is clearly jet-like in RL quasars, but may later expand roughly spherically (Furlanetto & Loeb 2001). In BAL quasars, outflows are likely to instead take the form of axisymmetric winds, accelerated by an unknown mechanism such as magnetrocentriful forces (*e.g.* Blandford & Payne 1982) or radiation pressure from lines (*e.g.* Proga, Stone, & Kallman 2000).

For a review of the observed relations between RL, BAL, and other quasars, the reader is referred to Antonucci (1991). For the purposes of this study however, the important point is only that the populations of quasars that are observed to host outflows are consistent with a random subset of all quasars, and that these outflows exhibit a variety of structures. In this case, we adopt the simplifying assumption that all quasars host outflows of material, with a kinetic energy input equal to some fraction, $_k$ 0.05, of the total bolometric energy released over the quasar lifetime (see §5.2 for justification of our choice of $_k$).

Furthermore, the source lifetime $t_{\rm dyn}$ 10^7 yr is generally shorter than other time scales under consideration. We can then approximate the energy injection as a point source explosion of energy E $_k L_{\rm bol} t_{\rm dyn}$. We shall assume the bubble evolves adiabatically and ignore energy losses due to radiative cooling, pdV work against the IGM, and gravity. We also ignore the Hubble expansion and peculiar velocities (including accretion infall), and assume that the bubble expands into a medium of uniform overdensity $_s$. The effect of relaxing these assumptions will be examined later.

3.1. *Outflow Scales*

Under these simplifications, the bubble behaves as a Sedov-Taylor blast (Sedov 1959) solution, which describes the adiabatic expansion of a hot sphere of plasma into cold medium. For our cosmological model, this gives a physical radius of

$$R_{\rm s} = \ _0 \left(\frac{Et^2}{\ }\right)^{1/5} = 1.7\,{\rm Mpc}\, E_{60}^{1/5}\ _{\rm s}^{-1/5}(1+z)^{-3/5} t_{\rm Gyr}^{2/5}; \qquad (10)$$

where E_{60} is the energy in the hot medium in units of 10^{60} ergs, $t_{\rm Gyr}$ is the expansion time of the bubble in Gigayears, the overdensity of the surrounding medium $_s$ is defined such that $_s = \ _b/\ _b$ (rather than $_b/\ _b - 1$) and $_o = 1.17$ for a $= 5/3$ gas (*e.g.* Shu 1992). Thus the shock velocity is $v_s = 2/5\, dR/dt = 1500\, R_{s,{\rm Mpc}}^{-3/2} E_{60}^{1/2}\ _{\rm s}^{-1/2}(1+z)^{-3/2}$ km s^{-1}, where $R_{s,{\rm Mpc}}$ R_s Mpc^{-1}. and, assuming a strong adiabatic shock, the postshock temperature is $T_s = (3\ m_p v_s^2)/(16 k_B) = 13.6 K v_s^2/({\rm km\ s^{-1}})^2$. We therefore obtain the temperature as a function of proper radius

$$T_{\rm s} = 3.1 \quad 10^7\,{\rm K}\, E_{60}\ _{\rm s}^{-1}(1+z)^{-3} R_{s,{\rm Mpc}}^{-3}. \qquad (11)$$

The functional form of this equation can be easily understood from $E \propto R_s^3 (k_B T_s)$ = constant, *i.e.* the blast wave conserves energy. As the postshock density $_{sh} = (\ +1)/(\ -1)\ _{\rm IGM}\ _{\rm s} = 4\ _{IGM}\ _{\rm s}$, for $= 5/3$, the postshock entropy can then be calculated as

$$S_{\rm s}(r) \quad \frac{T}{n_{\rm s}^{2/3}} = 1.8 \quad 10^4\,{\rm keV\,cm^2}\, E_{60}\ _{\rm s}^{-5/3}(1+z)^{-5} R_{s,{\rm Mpc}}^{-3}. \qquad (12)$$

Finally E_{60} can be related to the halo mass and merger redshift corresponding to a given quasar, by combining eqs. (1) and (4), yielding

$$E_{60} = 1.2 \times 10^{-4} f_b M_{12}^{5/3} (1+z). \quad (13)$$

4. CRITICAL ENTROPY

The simple model of entropy injection described above can be easily extended to capture the global spatial dependence of energy injection and cooling, which has not been considered in previous preheating models. The great advantage of considering entropy is that it is conserved during adiabatic processes such as subsonic compression and the Hubble expansion, and remains constant as long as radiative cooling is inefficient. Moreover, Oh & Benson (2003) pointed out that for $(1+z)^3 > 10$, the cooling time depends only weakly on density and is always greater than the Hubble time. Thus, gas that is shocked to entropies greater than a critical value can never cool, regardless of the densities to which it is compressed.

This can be most clearly understood if we write the cooling time as a function of temperature and entropy, rather than temperature and density. Using $S \equiv T/n^{2/3}$, the isobaric cooling time can be written as

$$t_{\rm cool} = \frac{(3/2) n k_B T}{n_e^2 \Lambda(T)} = S^{3/2} \left[\frac{3}{2} \frac{\mu}{\mu_e^2} \frac{k_B}{T^{1/2} \Lambda(T)} \right], \quad (14)$$

where for a fully ionized gas, $\mu = 0.62$, and $\mu_e = 1.18$. The quantity in square brackets is a function of temperature only, and the entropy only changes the overall normalization of the cooling time.

In the left panel of Figure 2, we plot the cooling time at a constant entropy as a function of temperature for $Z = 0.1 Z_\odot$ and $0.3 Z_\odot$, and $S_{100} \equiv S/(100\,{\rm keV\,cm^2}) = 1$. We use fits to the cooling function computed by Sutherland & Dopita (1993). Changing S_{100} slides the curves up and down the vertical axis, but does not change their shape. The cooling time has a deep minimum at $T_{\rm min} = 2.3 \times 10^5$K, where the cooling function peaks. Although this time can be shorter than $t_{\rm cool}(T_{\rm min})$ at high temperatures, when $\Lambda(T) \propto T^{1/2}$ due to free-free emission and $t_{\rm cool} \propto T^{-1}$, this only occurs if $T > 10^8$K. As such hot gas can only be retained in the potential wells of extremely massive clusters with $T_{\rm vir} > 10$ keV, we can safely ignore this regime.

Thus, if $t_{\rm cool}(T_{\rm min}) > t_H$, *the gas can never cool in a Hubble time, regardless of any subsequent expansion or compression.* Since $t_{\rm cool}(T_{\rm min}) \propto S^{3/2}$, this will occur for all entropies greater than some critical value $S_{\rm crit}$, given by

$$S_{\rm crit} = 280\,{\rm keV\,cm^2} (1+z)^{-1} \left[\frac{E(z)}{(1+z)^{3/2}} \right]^{2/3} \left[\frac{\Lambda(T_{\rm min})}{6.3 \times 10^{-22}\,{\rm erg\,s^{-1}\,cm^3}} \right]^{2/3}, \quad (15)$$

where $E(z) \equiv \sqrt{\Omega_m (1+z)^3 + \Omega_\Lambda}$. We plot this critical entropy, expressed in terms of $S_{100,{\rm crit}} \equiv S_{\rm crit}/(100\,{\rm keV\,cm^2})$ in the right panel of Figure 2.

The fact that the entropy floor seen in groups and clusters is greater than $S_{\rm crit}$ is no coincidence: all lower-entropy gas would have dropped out by radiative cooling. Indeed, it was this very fact which lead Voit & Bryan (2001) to suggest that radiative cooling could cause the observed entropy floor, although cooling alone could not be wholly responsible, since in the absence of preheating this would require massive overcooling in groups (*e.g.* Balogh et al. 2001; Oh & Benson 2003), and would result in entropies at large cluster radii that are much lower than observed (Voit & Ponman 2003). The fact that, at all radii, the observed entropy floor is not far *above* $S_{\rm crit}$; however, is likely to be a manifestation of strong feedback, as discussed in detail below.

4.1. *Spatial Distribution*

The presence of a critical entropy suggests that the IGM can be divided into two fractions, material that has been heated to above $S_{\rm crit}$ and is therefore unavailable for galaxy formation, and a cold phase at $T \sim 10^4$K where all memory of preheating has been erased. At this point an analogy with the well-known (McKee & Ostriker 1977) three-phase model of the interstellar medium (ISM) within galaxies is irresistible. In the ISM case, supernova explosions result in a three-component medium in which a large fraction of the Galactic volume is filled with hot, tenuous gas. The remainder of the cold gas is then divided into dense clouds in which star formation occurs, and a relatively cool intercloud medium that accretes onto the clouds that lie outside of hot bubbles.

In the cosmological case, the $S > S_{\rm crit}$ phase, the $T \sim 10^4$ phase, and the galaxies themselves play the roles of the supernova bubbles, the cool medium, and the dense clouds, respectively. Quasar outflows expand into the IGM, leaving behind heated regions in which no further structure formation can occur. In the cooler zones between these bubbles, gas accretion continues apace, resulting in the formation of continually larger structures. Finally, the gas within the galaxies themselves not only condenses to form stars, but also fuels supermassive black holes, seeding new bubbles of $S > S_{\rm crit}$ intergalactic material.

We are interested in the radius $R_{\rm heat}$ of the bubble that is heated above the critical entropy, $S > S_{\rm crit}$. To find this, we consider the sequence of adiabats through which the gas is shocked and invert eq. (12). This gives a proper radius of

$$R_{\rm heat} = 5.6\,{\rm Mpc}\, S_{100,{\rm crit}}(z)^{-1/3} E_{60}^{1/3} \Omega_{\rm s}^{-5/9} (1+z)^{-5/3}, \quad (16)$$

(17)

and a corresponding gas mass $M_{\rm b,heat} = (4\pi/3) R_{\rm heat}^3 \Omega_b \rho_{\rm s}$ of

$$M_{\rm b,heat}(z, M) = 4.6 \times 10^{12}\,{\rm M}_\odot\, S_{100,{\rm crit}}(z)^{-1} E_{60}^{-2/3} \Omega_{\rm s}^{-2/3} (1+z)^{-2}. \quad (18)$$

If we equate this to the total shocked mass as a function of time, $M_s(t)$, via equation (10), we can find the timescale on which this entire mass of gas is preheated. It can be quite long for low-redshift, energetic sources:

$$t_{\rm expand} = 20\,{\rm Gyr} S_{100,{\rm crit}}(z)^{-5/6} E_{60}^{1/3} \Omega_{\rm s}^{-8/9} (1+z)^{-8/3}. \quad (19)$$

Thus, even after the demise of the quasar population at low redshift, their hot bubbles continue to expand and encompass larger tracts of the IGM. We discuss this further in section 5.5.

Unlike the ISM case, the initial positions of these sources are not determined by baryonic physics or galactic dynamics, but rather by the underlying dark-matter distribution. In order to track the evolution of the hot baryonic component, then, we must combine our outflow modeling with the formation rate of massive dark matter halos. Thus, the average number of shells with $S \geq S_{\rm crit}$ impacting a random region of space with an overdensity of 1, at a redshift z can be computed by integrating over

the range of masses that contribute to the overall luminosity function at each redshift. This gives

$$\langle N_S(z)\rangle = \frac{1}{\rho_{b,0}} \int_z^{\infty} dz' \frac{dt'}{dz'} t_{\rm dyn}^{-1} \int_{M_{40}(z')}^{\infty} dM \; M_{b,\rm min}(z'; \delta_s; z; M) \frac{dL_B}{dM} [z'; L_B(z'; M)]; \quad (20)$$

where $\rho_{b,0}$ is the mean baryonic density at $z = 0$, $M_{40}(z')$ is the mass corresponding to a circular velocity of 40 km s^{-1}, which approximates the minimum mass that can form after reionization (*e.g.* Barkana & Loeb 2001), and

$$M_{b,\rm min}(z'; \delta_s; z; M) \equiv \min\left[M_{b,\rm heat}(1; z'; M); \frac{4}{3} \rho_b \delta_s R_s^3(z; z'; M) \right]; \quad (21)$$

accounts for the possibility that a given outflow may not have expanded to contain a mass $M_{b,\rm heat}$ by the final redshift z. The factor of $t_{\rm dyn}^{-1}$ accounts for the fact that the finite duty cycle of quasars implies that only a fraction $(t_{\rm dyn}/t_{\rm H})$ are visible at any given time; the overall number density of sources is a factor $(t_{\rm H}/t_{\rm dyn})$ higher than the observed number density of bright sources. Assuming that outflows are randomly distributed allows us to simply relate $\langle N_S(z)\rangle$ to the total mass fraction of gas shocked above $S_{\rm crit}$ as

$$\delta_S(z) = 1 - \exp\left[-\langle N_S(z)\rangle\right]. \quad (22)$$

As our model associates a mass and formation redshift with each quasar, it can be easily generalized to account for the *increased* number of $S > S_{\rm crit}$ outflows that impact the regions that later form into large galaxies and clusters, which is due to the fact that quasars tend to be biased towards the densest regions of space. In this case, the average number of such outflows impacting a region that forms a halo of mass M_f at a redshift z_f is

$$\langle N_S(z_f; M_f)\rangle = \frac{1}{\rho_{b,0}} \int_{z_f}^{\infty} dz' \frac{dt'}{dz'} t_{\rm dyn}^{-1} \int_{M_{40}(z')}^{\infty} dM \; M_{b,\rm min}[z'; \delta_s(z'; z_f); z_f; M] \; b(z'; M; z_f; M_f) \frac{dL_B}{dM} [z'; L_B(z'; M)]; \quad (23)$$

where b is a now a "bias factor" that accounts for quasar clustering and $\delta_s(z'; z_f)$ is the overdensity of the forming object at the time it encounters an outflow.

To compute b we employ an analytical formalism that tracks the correlated formation of dark matter halos. In this model, described in detail in Scannapieco & Barkana (2002), objects are associated with peaks in the smoothed linear density field, in the same manner as the standard PS approach. This formalism extends the standard method, however, using a simple approximation to construct the bivariate mass function of two perturbations of arbitrary mass and collapse redshift, initially separated by a fixed comoving distance (see also Porciani et al. 1998). From this function we can construct the number density of source halos of mass M that form at a redshift z at a comoving distance r from a recipient halo of mass M_f and formation redshift z_f:

$$\frac{dn}{dM}(M; z; r | M_f; z_f) = \frac{d^2n}{dM dM_f}(M; z; M_f; z_f; r) \left[\frac{dn}{dM_f}(M_f; z_f) \right]^{-1}; \quad (24)$$

where $\frac{dn}{dM_f}(M_f; z_f)$ is the usual PS mass function and $\frac{d^2n}{dM dM_f}(M; z; M_f; z_f; r)$ is the bivariate mass function that gives the product of the differential number densities at two points separated by an initial comoving distance r, at any two masses and redshifts. Note that this expression interpolates smoothly between all standard analytical limits: reducing, for example, to the standard halo bias expression described by Mo & White (1996) in the limit of equal-mass halos at the same redshift, and reproducing the Lacey & Cole (1993) progenitor distribution in the limit of different-mass halos at the same position at different redshifts. Note also that in adopting this definition we are effectively working in Lagrangian space, such that r is the *initial* comoving distance between the perturbations. Fortunately as shock propagation is likely to be more closely dependent on the column depth of material between the source and the recipient than on their physical separation, this natural coordinate system is more appropriate for this problem than the usual Eulerian one. We then define the bias factor as

$$b(z; M; z_f; M_f) = \frac{dn}{dM}(z; M; r \to \infty; M_f) \left[\frac{dn}{dM}(z; M) \right]^{-1}; \quad (25)$$

which is simply the number density of mass M, redshift z halos near the final object, divided by the average density of such halos. Finally for the effective radius, one works in Lagrangian comoving coordinates, such that r is the virial radius plus the radius which would contain $M_{b,\rm min}$ in a mean-density medium, $r = \left[\frac{3}{4\pi\rho_{b,0}} M_{b,\rm min}\right]^{1/3} + r_{\rm vir}(M)$. Note that this calculation of bias, while carried out within our merger formalism, depends only on the mass of the quasar host galaxy, the turn-on redshift for the quasar, and the mass and formation redshift of the final object. As these are the same quantities that arise in an approach based instead on accretion, one would expect the relationship between $\langle N_s(z_f; M_f)\rangle$ and $\langle N_S(M)\rangle$ to be similar in any such model. This means that the rough features derived below are likely to persist, regardless of the detailed physics of quasar generation.

To approximate δ_s, we appeal to the standard top-hat collapse model (see *e.g.* Peebles 1980), which relates the true overdensity to the "linear" overdensity, δ_L expressing both quantities parametrically in terms of a collapse parameter, θ; as

$$\delta_s(z; z_f) = \frac{9}{2} \frac{(\theta - \sin\theta)^2}{(1 - \cos\theta)^3}; \quad (26)$$

and

$$\delta_L(z; z_f) = 1 + \frac{3}{5} \left(\frac{3}{4}\right)^{2/3} (\theta - \sin\theta)^{2/3} = 1.69 \frac{D(z)}{D(z_f)}; \quad (27)$$

where $D(z)$ is again the linear growth factor.

Finally, we relate $\langle N(z_f; M_f)\rangle$ to $f_S(z_f; M_f)$; the fraction of objects with collapse redshifts z_f and mass M_f whose formation is suppressed by preheating by quasar outflows. As our formalism can only account for the correlations between two halos, we must adopt an approximation for the fraction of objects that are affected by multiple outflows. The simplest approach is to assume that while outflows only impact a fraction of the overall cosmological volume, their arrangement *within that fraction* is completely uncorrelated (as in Scannapieco, Schneider, & Ferrara 2003). In this approximation $f_S(z_f; M_f)$ and $\langle N_S(z_f; M_f)\rangle$

share the same relation as $_S(z)$ and $\langle N_S(z)\rangle$ in the average case, namely

$$f_S(z_f;M_f) = 1 - \exp[-\langle N_S(z_f;M_f)\rangle]: \quad (28)$$

We will adopt this *Ansatz* throughout this paper.

4.2. *Theoretical Uncertainties*

Before we apply the formalism developed above to derive the features expected in a model of strong feedback, we first pause to assess the uncertainties involved in our approach. Primary amongst these is our use of an adiabatic Sedov-Taylor solution for a point source explosion in a uniform medium. Here we note that

$$t_{\rm heat} \quad \frac{R_{\rm heat}}{v_{\rm sh}} = 4\,8 \quad 10^{10}\,{\rm yr}\,S_{100;{\rm crit}}^{-5=6}E_{60}^{1=3}{}_{\rm s}^{-8=9}(1+z)^{-8=3}; \quad (29)$$

which is larger than our source lifetime of t_o 10^7yr (as in equation 1) justifying our assumption of instantaneous energy injection.

Secondly, we ignored radiative losses. Since we are only interested in the early stages of the blast wave, when gas is shocked to high entropies ($S > S_{\rm crit}$) and can never cool, this is justified; $R_{\rm heat}$ is by definition the radius at which the cooling time of the gas is equal to the Hubble time. Beyond $R_{\rm heat}$, radiative cooling indeed becomes important and the evolution of the blast wave is no longer adiabatic.

Note that Compton cooling will dominate over collisional cooling at high redshifts ($z > 7$); however, we do not consider such high redshifts in our calculations: both the high IGM densities and the effectiveness of Compton cooling mean that the residual entropy is low. We also ignored the deceleration of the shock due to the $p\,dV$ work it does on the IGM, which is justified as long as $v_{\rm sh}^2$ $P_{\rm IGM}$, or $T_{\rm shock}$ $T_{\rm IGM}$ 10^4K, which is certainly the case. Gravitational deceleration is unimportant as long as the work done in sweeping up the shell out of the potential well $W = 0\,5\int_R {}_g\, d^3x = G\ M_{\rm halo}\ {}_{\rm IGM}R_{\rm sh}^2$ is smaller than the energy of the explosion, which it is

$$\frac{W(S > S_{\rm crit})}{E} = 4\,5 \quad 10^{-2}S_{100;{\rm crit}}^{-2=3}E_{60}^{-1=3}{}_{\rm s}^{-1=9}(1+z)^{-1=3}M_{12}: \quad (30)$$

Note that since E / $M_{12}^{5=3}$, W=E / $M_{12}^{1=6}$, so the dependence on halo mass is very weak. Finally, ignoring Hubble expansion is valid as long as $v_{\rm sh}$ $H(z)R_{\rm sh}$, which is only marginally valid:

$$\frac{v_{\rm sh}}{H(z)R_{\rm heat}} \quad \frac{t_{\rm heat}}{t_H} = 3\,5S_{100;{\rm crit}}^{-5=6}E_{60}^{1=3}{}_{\rm s}^{-8=9}(1+z)^{-7=6}: \quad (31)$$

Our model is therefore conservative in that we underestimate the extra kinetic energy associated with the Hubble expansion.

In order to use the Sedov-Taylor solution, we have assumed a point source explosion in a homogeneous medium, characterized by some mean overdensity . In fact, the density profile is more likely to be that of a power law; in addition the medium is not static but is being accreted by the halo. It might seem therefore that the dynamics of the explosion are no longer accurately described. In fact, Barkana & Loeb (2001) and Furlanetto & Loeb (2001) have constructed numerical models of outflows and solved the coupled system of differential equations to describe the outflow dynamics, modeling both the radial dependence of the density profile as well as accretion infall. They find remarkable agreement with a simple Sedov-Taylor type model such as that used here, which ignores the density profile and infall, as well as cooling, external pressure of the IGM, and the gravitational potential of the host halo (see Fig. 1 of Furlanetto & Loeb (2001), and associated discussion). This can be understood, since in all cases $R_{\rm heat}$ $R_{\rm vir}$, and the swept-up mass is dominated by that accumulated at large radii, when the density is close to the cosmological mean density. It is therefore largely independent of the details of the infall region.

We have completely bypassed the issue of how the quasar wind escapes from the host galaxy. Such issues are beyond the province of our semi-analytic model and can only be studied with hydrodynamic simulations. To our knowledge, there has been no detailed numerical study of quasar winds, although there is a significant body of literature on starburst winds (e.g., Strickland & Stevens 1999; MacLow & Ferrara 1999; Mori, Ferrara & Madau 2002; Fujita et al. 2003). Simulations of a centrally concentrated nuclear starburst most closely approximate quasar winds and generically find that starbursts punch a hole through the ISM of the galaxy ("blow-out"), venting most of the energy of the wind (with little radiative losses) while entraining little cold gas, which remains in the galaxy. Some fraction (few 10%) of the kinetic energy of the outflow can be radiated in internal, inward propagating shocks if there are significant off-nuclear supernova explosions (Mori, Ferrara & Madau 2002), but the radiated energy diminishes for a single, central energy source.

In fact, a single source, rather than smoothly distributed energy injection, is the most efficient means of quickly producing blow-away (Strickland & Stevens 1999). The coupling between the ISM and the wind diminishes rapidly for more energetic bursts, as blow-out becomes more efficient; only for very small dwarfs M_g 10^6M is a large fraction of the ISM entrained in the outflow (MacLow & Ferrara 1999). Blow-out would likely be particularly efficient for an initially bi-polar outflow such as an quasar wind. Thus, while an quasar wind has not been directly simulated, it certainly lies in the region of parameter space where energy should be efficiently delivered to the IGM. In any case, our model is only applicable once the wind has propagated out of the host galaxy: all uncertainty in energy loss within the host galaxy is encapsulated in the free parameter $_k$. For simplicity, we have assumed $_k$ to be independent of galaxy mass. We emphasize that our model only taps a very small fraction, $_k$ 5%, of the total available kinetic luminosity, and so preheating can still be important even if an appreciable fraction of energy is radiated away in the ISM of the host.

We approximate the metallicity of the IGM as $0\,1Z$, consistent with the level of pre-enrichment necessary to explain the lack of low-metallicity G-dwarf stars in the solar neighborhood (*e.g.* Ostriker and Thuan 1975), as well as in other large nearby galaxies (Thomas, Greggio, & Bender 1999). This should also be representative of the metallicity of regions surrounding quasar outflows at $z = 2$, when preheating by outflows peaks. Such regions now constitute the intracluster medium, which are observed to have metallicity Z $0\,3Z$; if 30% of all present-day stars have formed by z 2, as indicated by the Madau plot, then $Z(z = 2)$ $0\,1Z$. However, assuming a higher metallicity does not greatly alter $S_{\rm crit}$ (see Fig 2).

The greatest uncertainty is $_k$ L_k=$L_{\rm Bol}$, the fraction of the total bolometric luminosity (assumed to be the Eddington luminosity) which appears as kinetic luminosity. Most observations suggest that $L_{\rm k}$ $L_{\rm B}$ for both radio-loud (Willott et al 1999) and BAL quasars (Furlanetto & Loeb 2001), albeit with at least an order of magnitude uncertainty. Since L_B $0\,1L_{\rm Bol}$ (Elvis et al 1994), $_k$ $0\,1$ is reasonably motivated from observations.

However, the uncertainty is so large that we shall simply take $_k$ to be a free parameter, which we use to match the observed quasar luminosity function, as described in the following section.

5. IMPLICATIONS FOR STRUCTURE FORMATION

5.1. *Global Features*

From eqs. (24) and (28), we can construct the fraction of galaxies whose formation is suppressed given an arbitrary luminosity function $[z;L_{\rm B}(z;M)]$: Yet our model is not complete without correcting for the corresponding suppression in quasar formation. Naively, one might consider convolving the luminosity function with the fraction of objects affected by heating at a given redshift, replacing $[z;L_{\rm B}(z;M)]$ with $[1-f_S(z;M)]$ $[z;L_{\rm B}(z;M)]$: Yet this approximation would result in a severe underestimate, as in reality two galaxies of mass M=2 that formed at early times can still merge to ignite a quasar at z, even if the formation of additional galaxies of mass M is largely excluded at this redshift.

A better approach relies on the fact, as we shall see below, that $\langle N_S(z;M)\rangle$ is in general monotonically increasing with time. Thus we define an "exclusion redshift," $z_{\rm ex}(M)$ such that all M mass galaxies forming by $z_{\rm ex}(M)$ contribute to the quasar luminosity function, while later forming galaxies do not, with $z_{\rm ex}$ defined implicitly as

$$\langle N_S[z_{\rm ex}(M);M]\rangle = 1: \qquad (32)$$

With this definition, we then impose that for all halo masses and redshifts such that z $z_{\rm ex}(M_{\rm halo}$=2), eq. (6), gas can no longer cool and the supply of cold gas is shut off. Thus, only halos that formed at $z > z_{\rm ex}$ will contain cold gas to fuel quasars, and only their mergers need be considered. These progenitor galaxies will in general reside in a much larger host halo (such as a group or cluster), whose mass greatly exceeds the sum of the merging galaxy masses. Thus eq. (6) must be rewritten to include an additional integral over possible final masses, $M_{\rm big}$ of the final object. Defining $M^0_{\rm big} = M_{\rm big} - M_{\rm halo}$ this integral can be written as

$$(z;L_B) = \frac{3}{5\ _{\rm bh}}\frac{t_{\rm dyn}(z)}{5.73\quad 10^3 L\quad M^{-1}}\int_{0.25M_{\rm halo}}^{0.5M_{\rm halo}} d\ M_{\rm halo}$$
$$\frac{dn}{dM^0}(z_{\rm ex};M^0)\int_{M^0}^{1} dM^0_{\rm big}\frac{d\ ^{2^0}_{\rm big^0}}{dM^0_{\rm big}}$$
$$\Big\langle f_2\quad (z_{\rm ex});\ ^2(M^0);\ (z);\ ^{2^0}_{\rm big}\Big\rangle$$
$$\frac{d^2N_{\rm merge}}{d\ M_{\rm halo}dt}(z_{\rm ex};\ M_{\rm halo};z;M_{\rm big}): \qquad (33)$$

Note that here we assume that the galaxies contained in each sub-halo merge instantaneously as they fall into the larger halo $M_{\rm halo}$, and do not attempt to account for dynamical friction or tidal stripping within this region (*e.g.* Kauffmann, White, & Guiderdoni 1993; Cole et al. 1994; Somerville & Primack 1999) as these are beyond the scope of our simple model and would only obscure the processes in which we are interested. Note also that in the limit in which z_c ! z, f_2 approaches $[\ ^2(M^0) - \ ^{2^0}_{\rm big}]$ and thus eq. (33) reduces to eq. (6).

We then adopt an iterative approach to obtain $(z;L_B)$ and $\langle N_S(z;M)\rangle$ as a function of our feedback parameter $_{\rm k}$: first computing $\langle N_S(z;M)\rangle$ from the simple WL03 model, applying eq. (33) to correct the luminosity function, computing $\langle N_S(z;M)\rangle$ from this corrected function, and so on. In practice this convergence is very quick, arriving at a self-consistent solution within two cycles, although we iterate five times in the results presented below.

In Figure 3 we show the $\langle N_S(z_f;M_f)\rangle$ values that result from models with F = 1 and three different values of $_{\rm k}$. Here we choose $_{\rm k}$ = 0.05 as our fiducial model, simply because it provides the best fit to the quasar luminosity function, as discussed in §5.2. We then double and halve this value to examine the impact of varying the feedback efficiency on our modeling, resulting in the $_{\rm k}$ = 0.025 and $_{\rm k}$ = 0.10 models depicted in the lower panels. In all cases $\langle N_S(z_f;M_f)\rangle$ is a monotonically decreasing function of redshift, as assumed.

While in a self-similar, hierarchical model, preheating by progenitors would be independent of the final host halo mass scale, three features of quasar outflows break this self-similarity. As energy injection is a non-linear function of halo mass, $E \propto M_{\rm bh} \propto M_{\rm halo}^{5/3}$; feedback is a strongly increasing function of mass. Secondly, the presence of a critical entropy imposes a scale into the problem, as the number of supercritical outflows is self limiting, and thus does not greatly exceed one even for the largest objects. Finally, high mass objects are more strongly clustered, and therefore more likely to collapse out of preheated gas than low mass objects. The effect is similar to well-known fact that gas metallicity has a strong density dependence, and metals are likely to be clustered around the highest density peaks. Metals are likely to be a good tracer of gas entropy, and the two should exhibit similar spatial bias.

Thus for larger masses halos with $M_f > 10^{13}M$, $\langle N(z_f;M_f)\rangle$ is a relatively weak function of mass. This is because as $\langle N(z_f;M_f)\rangle$ 1; the further formation of galaxies is strongly suppressed, and these objects are heated primarily by high-redshift M M_f progenitors. In this limit the bias is well approximated by the Lacey & Cole (1993) progenitor distribution

$$b(M;z;M_f;z_f) = \frac{f[\ (z) - \ (z_f);\ ^2(M) - \ ^2(M_f)]}{f[\ (z);\ ^2(M)]}; \qquad (34)$$

where (z) and (z_f) are the "collapse thresholds" and $^2(M)$ and $^2(M_f)$ are the variances associated with the progenitor and final objects, respectively. As M M_f, $^2(M)$ $^2(M_f)$, and therefore eq. (34) is nearly independent of the M_f. In other words, the number density of $M < 10^{12}M$ progenitors is roughly equivalent for groups and massive clusters that form at the same redshift, and thus $\langle N(z_f;M_f)\rangle$ is largely equal for these objects.

Similarly, the impact of quasar heating on low-mass, $M < 10^{13}M$ objects has a very different dependency on the feedback parameter $_{\rm k}$ than at higher mass scales. While $N(0;10^{10}M\ )$ changes from 0.05 to 0.3 as $_{\rm k}$ goes from 0.025 to 0.10, $N(0;M > 10^{13}M\ )$ changes only from 2 to 4 for the same $_{\rm k}$ values. Again this is a manifestation of feedback effects, which are almost nonexistent in the $10^{10}M$ case, but greatly reduce the number of outflows generated by large galaxies. In fact, the true dependence of $N(0;M > 10^{13}M\ )$ on the feedback parameter is likely to be less, as eq. (33) applies the same correction to the luminosity function, regardless of the overall environment. In reality, $(z;L_B)$ should be somewhat more suppressed in clusters than the field, leading to an even weaker dependence of cluster preheating on $_{\rm k}$.

To explore these dependencies further, in Figure 4 we plot the contribution to $\langle N_S(z_f;M_f)\rangle$ from sources above some higher

redshift z_s, in our fiducial model. Here we see that in the higher-z_f, lower-mass objects, the impact of quasar halos is extremely weak at all times. One the other hand, in the $z_f = 0$, lower-mass objects, a substantial upturn in the contribution from sources at lower redshifts is seen, particularly in the $10^{10}M$ case. This is due to the ability of S $S_{\rm crit}$ winds from larger objects to move into underdense regions if given sufficient time to expand. Finally, at higher masses, a sizeable contribution to $\langle N_S(z_f; M_f)\rangle$ is observed at all redshifts, arising from progenitor objects.

From the values shown in Figure 3, we can directly calculate $z_{\rm ex}(M)$ as well as the fraction of suppressed galaxies, as computed from eq. (28). These are shown in Figure 5, again for three representative $_{\rm k}$ values. This plot provides a different perspective on the trends seen above. In our fiducial model, because $f_S(z_f; M < 10^{11}M$) 0.25 at all redshifts, low-mass galaxy formation continues largely unimpeded to this day. In the $10^{12}M$ to $10^{13}M$ mass range, however, a steep rise in $z_{\rm ex}$ take place as feedback becomes more effective. Finally, at masses $> 10^{13.5}M$; $z_{\rm ex}$ values are largely independent of mass, and strong feedback occurs in all cases. These trends persist in the $_{\rm k} = 0.025$ and $_{\rm k} = 0.10$ models although the overall values shift somewhat. In general, raising the feedback efficiency causes the transition region in $z_{\rm ex}$ to move to smaller masses, while pushing the high-mass $z_{\rm ex}$ plateau to higher redshifts.

5.2. *Entropy and the Quasar Luminosity Function*

The trends seen in Figure 5 have a direct impact on the B-band quasar luminosity function, as shown in Figure 6. From this plot it is immediately clear that the exclusion of z $z_{\rm ex}$ objects in our fiducial models provides an excellent fit to the data. Less clear is just how much of this agreement is due to our allowing ourselves a specific choice of $_{\rm k} = 0.05$:

We would maintain that the best answer to this question is exactly half. There are two characteristic values that appear in this figure, the first of which is the characteristic luminosity, or mass, above which feedback effects are imprinted. This corresponds to the transition region in Figure 5, which we saw could be simply shifted to higher (lower) values by decreasing (increasing) $_{\rm k}$. Yet increases in the kinetic-energy input also have the effect of pushing $z_{\rm ex}$ to higher redshifts.

This corresponds to the second characteristic value in Figure 6, namely the redshift at which feedback corrections to the WL03 model become important. This value is not arbitrary within our model, but rather is fixed when $_{\rm k}$ is chosen to reproduce the characteristic L_B. Thus the $_{\rm k} = 0.025$ model shown in this figure not only fails to halt the formation of a sufficient number of higher-luminosity quasars at $z = 0.25$, but fails to have any impact whatsoever at z 1.25: Similarly, the $_{\rm k} = 0.10$ model both over-estimates feedback effects at $z = 0.25$, and deviates from the WL03 model too soon.

5.3. *A Heuristic Aside*

To gain a heuristic understanding of our results, it is useful to explore a Soltan-type argument (Soltan 1982; Yu & Tremaine 2002), relating the accretion history of black holes to their total energy release over the history of the universe. We can simply modify the argument to consider the total entropy injected into the IGM, rather than the total optical light emitted. To do so, we note from eq. (18) that $M_{\rm b;heat} / E_{60} = {}_{\rm k}L_{\rm bol}t_{\rm dyn} = {}_{\rm k\ rad}M_{bh}c^2t_{\rm dyn} = {}_{\rm k\ rad}\ M_{\rm\ bh}c^2$. Here, the radiative efficiency is $_{\rm rad}$ $L_{\rm bol}=(\dot{M}c^2)$ 0.1 from comparing estimates of the local black hole mass density with the quasar luminosity function from the 2dF redshift survey (Yu & Tremaine 2002). Thus, the total mass density of gas heated above $S_{\rm crit}$ is directly proportional to the mass density in black holes, if we ignore the time delay due to the finite bubble propagation speed. Specifically, we obtain

$$_b(S > S_{\rm crit}) \quad 10^4\ {}_{\rm bh}S_{100;{\rm crit}}(z)^{-1}(1+z)^{-2\ -2=3}_{\ s}\ \frac{k}{0.05}\ \frac{\rm rad}{0.1}\ : \qquad (35)$$

The comoving mass density in black holes as a function of redshift is

$$_{\rm bh}(z) = \int_z^{\ 1} dz' \int_0^{\ 1} dL_B \frac{L_{\rm bol}}{_{\rm rad}c^2}\ (L_B; z')\frac{dt}{dz'}: \qquad (36)$$

We can use eqs. (35) and (36) to obtain $_b(S > S_{\rm crit}; z)$, without recourse to Press-Schechter theory. We can also approximately understand the exclusion redshift $z_{\rm ex}$ from the fact that the highest density peaks are always the first to be polluted to high entropy, just as they are also always the first to be polluted to high metallicity. The exclusion redshift can therefore be approximated by:

$$f(S > S_{\rm crit}) = \frac{_b(S > S_{\rm crit})}{_b} \quad \text{erfc}\ \frac{c}{\sqrt{2}\ (M; z_{\rm ex})}\ : \qquad (37)$$

From this we can understand the evolution of the mass suppression scale. Often in models of structure formation, the suppression mass (for instance, the Jeans mass) is self-regulating and therefore traces the non-linear mass scale (e.g., Chiu & Ostriker 2000). This is manifestly not the case for preheating. For instance, if preheating affected only 2 perturbations, then $f(S > S_{\rm crit})$ 0.05, independent of redshift. Instead, from the sharp rise in the black hole mass density with time, we know that $f(S > S_{\rm crit})$ increases with time. Thus, at late times, preheating affects progressively smaller perturbations: from 6 perturbations at z 5 ($M_{\rm suppress}$ $10^{13.5}M$) to 1 perturbations at z 1 ($M_{\rm supress}$ $10^{12}M$). Once preheating affects the bulk of halos, the supply of cold gas is cut off and the comoving luminosity density in quasars and star formation abruptly drops.

5.4. *Entropy and Galaxy Formation*

In Figure 7 we compare our feedback models with what has emerged as one of the most widely-used quantifiers of galaxy evolution, the comoving space density of the star formation rate, $_?$: In this plot, the barrage of multi-wavelength observations illustrates that $_?$ rises by an order of magnitude between $z = 0$ and $z = 1$; and evolves much more slowly at higher redshifts. For reference, we also include the analytical model given by eq. (2) of Hernquist and Springel (2003), with a normalization of $_?(0) = 0.04M$ yr^{-1} Mpc^{-1}:

While it is still unclear whether the evolution of $_?$ reaches a peak around z 1.5 (*e.g.* Madau et al. 1996) or stays flat to much higher redshifts, the primary uncertainties in this comparison are theoretical rather than observational. A rough estimate of the number of stars resulting from starbursts can be taken by simply evaluating the time derivative of the total mass contained in galaxies, scaled to the average number of stars formed in each burst. This gives

$$_?(z) = f_? \frac{_b}{_0} \frac{dz}{dt} \int_{M_{40}(z)}^{\ 1} dM \frac{dn}{dMdz}\ 1 - f_S(z; M)\ ; \qquad (38)$$

where $f_?$ is a "star formation efficiency" that parameterizes the fraction of gas in a given starburst that is converted to stars. Taking $f_?$ to be a free parameter that we match to observations at high redshifts yields the solid line shown in this figure. Obviously the fall-off at lower redshifts is much more severe than observed, yet the reason for the discrepancy is clear, as the majority of observed low-redshift star formation occurs not as bursts, but rather though quiescent star formation in disk galaxies (*e.g.* Tan, Silk, & Balland 1999).

This sort of star formation could simply be modeled by a term that depends on the total (integral) mass in galaxies

$$_?{}_{\rm quiescent}(z) = f_{?\,_l} \frac{r_{\rm vir}}{v_c}(z) \frac{b}{0} \int_z^{\;1} dz' \int_{M_{40}(z')}^{\;1} dM \frac{dn}{dM dz'} \left[1 - f_S(z';M)\right] \; ; \quad (39)$$

where the dynamical time $(r_{\rm vir}=v_c) = 30 t_{\rm dyn}$ as given by eq. (1) and $f_{?\,_l}$ is now a parameter that determines the average rate of quiescent star formation in disks. Adding this contribution (with $f_{?\,_l} = 0.003$) to eq. (38) results in the dashed line shown in Figure 7. While this provides a reasonable fit to observations, the necessary introduction of a second free parameter makes this comparison a bit unsatisfying. We can conclude only that $_?(z)$ measurements are consistent with strong-feedback models, although they do not provide particularly strong constraints. We note in passing, however, that our fiducial $_{\rm k} = 0.05$ model is consistent with observations of Lyman-break galaxies at $z \quad 3$, as only halos of $M > 10^{13} M$ have $z_{\rm ex} \quad 3$, while Lyman-break galaxies are thought to reside in halos with masses $10^{12} M$, or even less (*e.g.* Scannapieco & Thacker 2003).

A more rigorous confrontation with observations arises from restricting our attention to the subset of galaxies in which quasar feedback has the strongest impact, namely those with masses $> 10^{12} M$. Thus in Figure 8 we plot the number density of the most luminous galaxies at three representative redshifts. Here we restrict our attention to K_s measurements as taken by Pozzetti et al. (2003), as such infrared measurements are most sensitive to the overall galaxy stellar masses, rather than a combination of stellar masses and formation histories (*e.g.* Madau, Pozzetti, & Dickinson 1998).

To convert our mass function to K-band magnitudes in an approximate and simple manner we make use of the Tully-Fisher relation observed by Pierini & Tuffs (1999), which relates the K^0-band absolute magnitude and circular velocities of disk galaxies as

$$M_{K^0} = -9.66\, v_c - 1.41 : \quad (40)$$

For purposes of this comparison, we associate v_c in this equation with the underlying halo circular velocity, making no attempt to correct for galaxy morphology or differences between K^0 and K_s bands. This allows us to compute the luminosity function as

$$_{K_s}(z) = \int_z^{\;1} dz' \frac{dv_c}{dK_s} \frac{dM}{dv_c} \frac{dn}{dM dz'} \left[1 - f_S(z';M)\right] \; ; \quad (41)$$

where M is a function of z' that is fixed by eqs. (40) and (2). This is shown as the solid ($_{\rm k} = 0.05$) and short-dashed ($_{\rm k} = 0.025$; $= 0.10$) lines in Figure 8.

Here we see that our simple model provides an excellent fit to the data, so much so that some degree of chance must be involved, given the uncertainties. This agreement is even more striking given the large *inconsistencies* between the data and the more detailed galaxy-formation models compiled from Menci et al. (2002), Cole et al. (2000), and Kauffmann et al. (1999) in this figure, particularly for the brighter objects. Furthermore, this sample is by no means the only one that illustrates a discrepancy between observations and modeling. Rather, a large number of independent surveys are consistently pointing to a lack of galaxy evolution below $z < 1.5$: (*e.g.* Cimatti et al. 2002; Chen et al. 2003a; Glazebrook et al. 2003; Somerville et al. 2003), which appears to present a "paradox" for current hierarchical models (*e.g.* Chen et al. 2003b). Given this well-known discrepancy, is it not perhaps the case that we obtain agreement by overlooking an important piece of galaxy-formation physics that when accounted for would completely change our model?

While a key issue in galaxy formation has indeed been neglected, we would suggest that this points not to a shortcoming in our approach, but rather to its greatest strength. Despite their diversity, the literature models compiled in this plot share the same core mechanism for arriving at the characteristic luminosity ($L^?$), above which the number densities of galaxies falls off precipitously. Typically this is associated with a post-viralization cooling condition (Rees & Ostriker 1977; Dekel & Silk 1986), which arises when adopting a picture in which gas is shocked to the virial temperature at the redshift of halo collapse, and then must have time to cool into a disk before star-formation can occur. This can be implemented by enforcing some variation on the condition

$$f\, t_{\rm cool}(M; z_{\rm col}) \quad t_{\rm obs} - t_{\rm col} ; \quad (42)$$

where $t_{\rm obs}$ is time corresponding to the redshift of observation, and $t_{\rm cool}(M; z_{\rm col})$ is the cooling time as calculated from eq. (14) assuming a density of 180 times the mean density at $z_{\rm col}$ and a temperature equal to the viralization temperature $T_{\rm vir} = 35 K [v_c/({\rm km\,s^{-1}})]^2$:

At the lowest redshifts, this condition provides a similar and equally good fit to the data as our modeling, as illustrated in Figure 9. In the upper left panel of this plot, we see that f can easily be chosen to exclude star-formation in a similar subset of halos as quasar feedback. Yet once f is fixed, the imposition of a post-virialization cooling condition has a very different impact on higher-redshift halos.

Although the $(1+z)^3$ increase in the mean density shortens higher-redshift cooling times, this effect is somewhat counteracted by the strong $t \;/\; (1+z)^{3/2}$ dependence on time with redshift. This means that in higher-redshift objects, eq. (42) continues to enforce a substantial redshift delay (z) between the halo collapse and star formation redshifts. Thus, the reduction in objects with luminosities $L_?$ at $z = 0$ is achieved *as a result* of a strong redshift evolution in their number densities. This generic feature, while lessened somewhat by more complicated modeling, is the primary source of the discrepancy between the observations and standard models.

Furthermore, the imposition of a post-virialization cooling criterion fails quantitatively in comparison with numerical simulations. If no feedback or preheating is invoked, high-resolution simulations predict that $30 - 40\%$ of the gas in clusters should cool (Suginohara & Ostriker 1998; Lewis et al. 2000; Davé et al. 2001). This is because while $t_{\rm cool} > t_H$ at the virial radius, $t_{\rm cool} \quad t_H$ in the dense inner regions of clusters, resulting in catastrophic cooling. By contrast, K-band observations indicate a cold gas fraction of $5 - 10\%$ in most groups

and clusters, independent of virial temperature. A lucid recent discussion of this overcooling problem is given in Balough et al. (2001).

On the other hand, our proposed feedback criterion differs from the customary one in that it is evaluated not at the virial radius but at the dense centers of halos (which are the most highly biased and therefore most likely to have been preheated). Quasar feedback excludes a fixed fraction of galaxies within halos of a given mass and formation redshift, regardless of the redshift at which they are observed. Thus the solid and dotted lines in Figure 9 remain fixed at all redshifts, evolving only to enforce $z_{\rm col} \quad z_{\rm obs}$ at the small-mass end. This results in the observed lack of evolution seen in Figure 8, which naturally reproduces the observations using only a simple transformation between v_s and M_{K_s} :

Our point is not that a lack of $z < 1.5$ evolution can not be accommodated in standard galaxy-formation scenarios, but rather that this behavior can be reproduced only by including a series of detailed corrections. In galaxy formation models regulated by quasar feedback, this lack of low-redshift galaxy evolution emerges naturally, imposed by the redshift at which preheating becomes prevalent, which in turn is fixed by the observed value of $L_?$.

5.5. *Entropy, Clusters and the Intergalactic Medium*

Clearly, the presence of quasar outflows has implications far beyond the formation rate of supermassive black holes and the regulation of star formation in the galaxies that surround them. In fact, as described above, the most-clearly observed imprint of non-gravitational heating on cluster scales is not on galaxies themselves, but rather on the diffuse intracluster medium (Kaiser 1991). The implementation of strong quasar feedback as in Figure 3 naturally results in an increase in ICM entropy, placing it on a higher adiabat that prevents it from reaching a high central density during collapse, which in-turn decreases its X-ray luminosity (*e.g.* Tozzi & Norman 2001). Furthermore for a fixed level of heating per gas particle, this effect is more prominent for poorer clusters, whose virial temperatures are comparable to this extra contribution. As a result, a $T^{7/2}$ relation is established in hot systems and broken for colder systems, reconciling observations with semi-analytical studies and numerical simulations by establishing a fixed entropy "floor" of $55 - 110\, h^{-1/3}$ keV cm^2.

A further constraint on the state of ICM gas comes from measurements of the cosmic microwave background (CMB). As CMB photons are relatively low-energy, thermal motions in hot ionized regions are able to scatter them to higher energies: increasing the number of energetic photons and reducing the number of lower-energy ones. The magnitude of this shift is proportional to the Compton-y parameter, the temperature of the gas convolved with the total column density along a line-of-sight, and is thus most severe along sight-lines that pass through the hot and relatively dense ICM. This so called Sunyaev-Zel'dovich effect (Sunyaev & Zel'dovich 1972) has been well studied theoretically (*e.g.* Aghanim et al. 1997; Refregier et al. 2000) and detected in a number of clusters (*e.g.* Grego et al. 2001; Reese et al. 2002). The possibility of detecting the Sunyaev-Zel'dovich effect from galactic and quasar outflows has been explored by previous authors (Natarajan & Sigurdsson 1999; Yamada et al. 1999; Aghanim, Balland, & Silk 2000; Majumdar, Nath, & Chiba 2001; Platania et al. 2002), and the high optical depth measured by WMAP indicates that it might even arise from very high redshift sources $z > 10$, where Compton cooling is extremely efficient (Oh, Cooray, & Kamionkowski 2003).

Similarly, the $S \quad S_{\rm crit}$ regions that preceded clusters, while more difficult to measure individually, are likely to have left a substantial imprint on the global structure of the microwave background. In the upper panel of Figure 10, we plot the mean number of $S \quad S_{\rm crit}$ outflows impacting an arbitrary point in space, $\langle N_S(z)\rangle$, as estimated from eq. (22). Here we see that IGM heating is extensive for all three models under consideration, impacting $> 50\%$ of the mass before the $z < 1.5$ epoch of cluster formation, even in the lowest-energy, $_{\rm k} = 0.025$ case.

We can estimate the overall CMB distortions from these regions as

$$y(z) = \frac{_T c}{m_e c^2} \int_z^{z_{\rm max}} dz' \frac{dt}{dz'} kT(z') n_e(z') = 2.4 \quad 10^{-6} \int_z^{z_{\rm max}} dz' \frac{T_{\rm keV}(z')(1+z')^2}{E(z')} \langle N_S(z')\rangle; \quad (43)$$

with $T_{\rm keV}(z) \quad \frac{S}{100{\rm keV\,cm^2}} 8.7 \quad 10^{-3}(1+z)^{2 \quad 2/3} \quad 5.2 \quad 10^{-2} \frac{S_{\rm crit}(z)}{100{\rm keV\,cm^2}}(1+z)^2$, where we assume that mean heated regions are heated to levels slightly higher than $S_{\rm scrit}$ and $= 4$, such that $S^{2/3} \quad 4 S_{\rm crit}(z)$. While $y(z)$ is plotted in the central panel of Figure 10 over the full range of redshifts under consideration, note that only the present day value, $y(0)$, is accessible to observation. For all models, this value is well-below the observational limit on the total Compton distortion (Fixen 1996), but comparable to the 10^{-6} estimates of the total impact from gravitationally heated gas (*e.g.* Refregier et al. 2000). Thus more detailed comparisons between future CMB measurements and outflow models are likely to be able to place strong constraints on the overall level of quasar feedback.

In the lower panel of Figure 10 we turn our attention to even more diffuse regions of space, with overdensities of only a few. In order to estimate the impact of quasar winds of such circumgalactic gas, we modify eq. (24) as

$$\langle N_{S;{\rm cgm}}(z)\rangle = \frac{1}{b;0} \int_z^1 dz' \int_{M_{40}(z')}^1 dM \quad (44)$$
$$M_{\rm b;min}\{z'; [z';z_{\rm cgm}(z)];z;M\}$$
$$b[z';M;z_{\rm cgm}(z);M_{40}(z)] \frac{dL_B}{dM} [z;L_B(z;M)];$$

where now $z_{\rm cgm}(z) < z$ is chosen such that at a redshift z the region under consideration has ceased to expand, but has not yet collapsed into a bound structure, which can be achieved by requiring a "turn-around overdensity" associated with a collapse parameter $=$ in eqs. (26) and (27). Finally we take $M_{40}(z)$ as a rough estimate of the the typical Jeans mass in the post-reionization IGM (Barkana & Loeb 2001).

Surprisingly, only about 5% of the circumgalactic gas has been impacted by outflows at $z \quad 2$, but the fraction of heated gas increases to $30 - 40\%$ at $z \quad 0$. This may seem surprising, since the quasar population peaks at $z \quad 2$, after which the comoving density of sources falls sharply. The reason is the finite travel time of the bubbles, as given by equation (19). Thus, while the winds affect the sites of massive galaxy and quasar formation (which are highly clustered) early on, they only impact the low density IGM at late times. In particular, while quasar feedback has a large impact on the collapse of non-linear structures, its impact on the $5, z > 2$ regions associated with

the Lyman- forest is expected to be small. The feedback assumed in our modeling is therefore completely consistent with the observed properties of this material, although it remains that specialized analyses may be able to detect (or rule-out) its presence.

At lower redshifts, the circumgalactic gas acquires temperatures that tend to be described as "warm-hot." In fact, numerical simulations have shown that by $z = 0$ a large fraction ($30-40\%$) of baryons have been gravitationally heated to temperature of order 10^5-10^7 K, and that this warm-hot intergalactic medium (WHIM) extends into areas with overdensities of only a few (*e.g.* Cen & Ostriker 1999; Davé et al. 2001). At $z = 0$ Davé et al. (2001) find the temperature of this gas to be $10^{5.5}$ in 5 regions (see also Nath & Silk 2001). Taking $S_{\rm crit} = 150$ keV and 5 in the 50% of the circumgalactic gas impacted by quasar outflows by z 0 results in a similar value. Thus quasar feedback represents an energy source that is comparable to gravitational heating in the WHIM and is likely to have a large impact on its properties. Indeed, if production of the WHIM via quasar outflows is important, then the majority of the IGM will not be graviationally shocked at late times, but instead evolve isentropically. While observational constraints on this material are relatively weak at the moment, as in the CMB case, future studies are likely to provide a sensitive probe into heating of this mutiphase gas (*e.g.* Shull, Tumlinson, & Giroux 2003) and the impact of quasar feedback.

5.6. *Relation to Baryonic Stripping*

Finally, we relate the entropy-driven process of quasar feedback to the effects of starburst-driven winds. While previous work (Scannapieco, Ferrara, & Broadhurst 2000; Thacker, Scannapieco & Davis 2002) has shown that dwarf outflows are relatively inefficient at heating gas to S $S_{\rm crit}$ levels, they are nevertheless able to impede the formation of galaxies with masses $10^9 M$, through the transfer of momentum. In this case an SN driven shock accelerates the baryons in a neighboring perturbation to above their escape velocity, stripping them entirely from their associated dark matter and halting their collapse. Setting the mass of the perturbation times its escape velocity equal to the impinging momentum gives a rough estimate as to when such "baryonic stripping" will take place:

$$M_{\rm b,p} v_{\rm p} \quad (M_{\rm s} v_{\rm s}) \quad \frac{R_{\rm p}^2}{4 R_{\rm s}^2} \quad ; \qquad (45)$$

where $M_{\rm b,p}$, and $R_{\rm p}$ are the baryonic mass and radius of the perturbation, while $v_p = \sqrt{GM_{\rm p}/(2R_{\rm p})}$, with M_p the total mass of the perturbation. Relating M_s and R_s to E_{60} through eq. (10) and solving for the (physical) radius within which baryons will be stripped yields

$$R_{\rm strip} = 35\,{\rm Mpc}\, E_{60} \frac{s}{5=3} M_{12}^{-4=3} (1+z)^{-2} ; \qquad (46)$$

where $_s$ and $_p$ are the average overdensity of the expanding shock and the perturbation respectively, and M_{12} is the mass of the perturbation in units of $10^{12} M$: We can therefore include baryonic stripping in our modeling of quasar feedback by rewriting eq. (24) to account for the interactions in which $R_{\rm strip}$ R $R_{\rm heat}$. This gives

$$M_{\rm b,strip}(z^0; {}_s; z; M) \quad \min \max \left[M_{\rm b,heat}(1; z^0; M) ; \right. \qquad (47)$$
$$\left. \tfrac{4}{3} {}_b {}_s R_{\rm strip}^3(z^0; M) \right] ; \tfrac{4}{3} {}_b {}_s R_s^3(z; z^0; M) \quad ;$$

where we estimate $_p = {}_s$ 3. The resulting $z_{\rm ex}$ curves are shown in the upper panel of Figure 11 for our fiducial ($F = 1$, $_{\rm k} = 0.05$) model. Here we see that, due to the strong clustering and high masses of most quasar sources, baryonic stripping has an impact only on late-forming low-mass halos, while S $S_{\rm crit}$ heating dominates for objects with masses $> 10^{12} M$. Furthermore, such events occur well after the typical formation redshift of these small halos, and thus have a negligible impact on the quasar luminosity function as shown in the lower panels of this figure. Thus lower-redshift quasar feedback is completely different in nature from high-redshift SN driven-starbursts, and is driven almost exclusively by S $S_{\rm crit}$ heating.

6. DISCUSSION

In this work, we have considered the impact of quasar outflows on cosmological structure formation on all scales. By associating only a tiny fraction of a quasar's bolometric energy with an outflow of the form observed in radio jets or broad-absorption-line winds, we have shown that such objects can drastically transform our picture of the $z < 2$ universe, resolving a number of long-standing issues.

Quasar feedback ties together the densest objects at the center of galaxies with the most diffuse regions of intergalactic gas, impacting all intermediate structures much as SN explosions impact all environments within the interstellar medium. As outflows heat large regions of the IGM to entropies above $S_{\rm crit}$, they regulate their own formation, resulting in the observed fall-off in the number density of quasars below z 2. On larger scales, quasar feedback halts the formation of $M > 10^{12} M$ galaxies, providing an alternative mechanism for regulating galaxy formation than the usually-imposed condition of post-virialization cooling. Furthermore, while $L_?$ is fixed in a standard picture only as a result of strong redshift evolution, this value appears in a feedback model as the nonlinear mass scale at the redshift at which quasar outflows heat the denser regions of gas to S $S_{\rm crit}$ values. Thus the observed lack of $z < 1.5$ galaxy evolution, while arising only though detailed corrections in a standard picture, is a general and unavoidable feature of a model regulated by quasar feedback.

On intergalactic scales, feedback heats the denser regions of gas to values just above $S_{\rm crit}$, providing a natural explanation for why the ICM of clusters of all sizes has been generally preheated to entropy values *just above* the minimum excess observable. Furthermore, while the strong clustering of quasars precludes them from having a serious impact on the somewhat overdense $z > 2$ regions associated with the Lyman- forest, their global impact may provide us with sensitive observational probes through Compton distortions in the CMB and the multiphase structure of the ($z = 0$) WHIM.

While in a self-similar, hierarchical model, preheating by progenitors would be independent of the final host halo mass scale, there are three major features of quasar outflows that break this self-similarity. The first is that energy injection is a non-linear function of halo mass, $E \propto M_{\rm bh} \propto M_{\rm halo}^{5=3}$; which causes the largest objects to be most impacted. Secondly, the presence of a critical entropy imposes a scale into the problem, as the number of supercritical outflows is self limiting, and thus does not greatly exceed one even for the largest objects. Finally, high mass objects are more strongly clustered, and therefore more likely to collapse out of preheated gas than low mass

objects. A useful analogy is that of metallicity: the most overdense regions will tend to be polluted to high metallicity and high entropy first.

The three-phase (McKee & Ostriker 1977) model so much revolutionized our understanding of the interstellar medium that it naturally lead to widespread interest in galaxy formation though intergalactic shocking from starbursts (*e.g.* Ostriker & Cowie 1981) and even "quasar explosions" (Ikeuchi 1981). While we now believe structure formation is driven instead by dark-matter gravitational collapse, is there not a role for outflows in structure *regulation*?

Today, evidence for feedback effects from high-redshift starburst galaxies is better described as overwhelming than mounting. Analyses of C IV lines in quasar absorption spectra uncover an IGM that has been widely and inhomogenously enriched with stellar material (*e.g.* Cowie et al. 1995; Rauch, Haehnelt, & Steinmetz 1997) out to very high redshifts (Songaila 2001) and turbulently "stirred" at z 3 (Rauch, Wallace, & Barlow 2001). Large numbers of outflowing starbursts have been directly detected, both in optical and infrared observations at $3 < z < 4$ (Pettini et al. 2001) and in optical observations of lensed galaxies at $4 < z < 6.5$ (Frye, Broadhurst, & Benitez 2002; Hu et al. 2002). Furthermore it is clear from both analytical and numerical studies that these winds have an important effect on the gas in growing pre-virialized density perturbations, accelerating their baryons above the escape velocity and thereby regulating the formation of further such dwarves.

At the same time, evidence of similar feedback effects at low redshift is staring us in the face. At z 2 a large number of highly-clustered quasars are observed to be pummeling the denser regions of space, providing a natural energy source for the substantial preheating detected in X-ray observations of galaxy groups and clusters at z 0. These *are* the collapsed gaseous halos that have failed to form into galaxies, and they look nothing like the post-virialization clouds posited in standard scenarios. Can we really expect non-gravitational heating to be the primary driver of their properties and yet have played only a secondary role in the formation history of large galaxies?

As surveys scour the sky, reconstructing the history of galaxy formation in our universe, they only serve to highlight the interdependence between these star-forming regions and the diffuse gas that surrounds them. Similarly, a large range of numerical studies have suggested that there is more to the thermal and accretion history of the IGM than we had first imagined. By complementing galaxy surveys with detailed measurements of Compton distortions in the CMB, probes into the structure of the low-redshift WHIM, and perhaps even specialized analyses of the Lyman- forest, this history is accessible to us. Far from an abstract conjecture, quasar-regulated structure formation provides a clear and testable alternative to current low-redshift modeling, a postulated missing link that may soon be unearthed by multi-wavelength excavations into our cosmic past.

We are grateful to Arif Babul, Emanuele Daddi, Andrew King, Hui Li, Jaron Kurk, Crystal Martin, Daniel Proga, Volker Springel, Rob Thacker, Dmitri Uzdensky, Mark Voit, and J. Stuart Wyithe, as well as an anonymous referee for helpful comments and suggestions. This work was supported by the National Science Foundation under grant PHY99-07949.

REFERENCES

Aghanim, N., deLuca, A., Bouchet, F. R., Gispert, R., & Puget, J. L. 1997, A&A, 325, 9
Aghanim, N., Balland, C., & Silk, J. 2000, A&A, 357, 1
Antonucci, R. 1993, ARA&A, 31, 473
Arnaud, M. & Evrard, E. 1999, MNRAS, 305, 613
Babul, A., Balogh, M.L., Lewis, G.F., & Poole, G.B. 2002, MNRAS, 330, 329
Bahcall, J. N., Kirhakos, S., Saxe, D. H., & Schneider, D. P. 1997, ApJ, 479, 642
Balogh, M.L., Babul, A., & Patton, D.R., 1999, MNRAS, 307, 463
Balogh M. L., Pearce F. R., Bower R. G., & Kay S. T. 2001, MNRAS, 326, 1228
Barger, A. J., et al. 2003, ApJ, 584, L61
Barkana, R., & Loeb, A. 2001, Phys. Rep., 349, 125
Barnes, J. E., & Hernquist, L. 1992, ARA&A, 30, 70
Benson, A. J., & Madau, P. 2003, MNRAS, 344, 835
Bialek J. J., Evrard A. E., & Mohr J. J. 2001, ApJ, 555, 597
Blandford, R. D., & Znajek, R. L. 1977, MNRAS, 179, 433
Blandford, R. D., & Payne, D. G. 1982, MNRAS, 199, 883
Borgani, S., Governato, F., Wadsley, J., Menci, N., Tozzi, P., Lake, G., Quinn, T., & Stadel, J. 2001, ApJ, 559, 71
Boroson, T. A., & Meyers, K. A. 1992, ApJ, 397, 442
Briggs, F. H., Turnsheck, D. A., & Wolfe, A. M. 1984, ApJ, 287, 549
Brighenti, F., & Mathews, W. G. 2001, ApJ, 553, 10
Bromley, J. M., Somerville, R. S., & Fabian, A. C. 2003, MNRAS, submitted (astro-ph/0311008)
Cavaliere, A., Menci, N., & Tozzi, P. 1998, ApJ, 501, 493
Cavaliere, A., Menci, N., & Tozzi, P. 1999, MNRAS, 308, 559
Cen, R., & Ostriker, J. P. 1999, ApJ, 514, 1
Chen, H.-W., et al. 2003a, ApJ, 586, 745
Chen, H. W., et al. 2003b, in Multiwavelength Mapping of Galaxy Formation and Evolution, eds. R. Bender & A. Renzini (Berlin: Springer-Verlag)
Chiu, W.A., & Ostriker, J.P. 2000, ApJ, 534, 507
Cimatti, A. et al. 2002, A&A, 391, L1
Ciotti, L., & Ostriker, J. P. 1997, ApJ, 487, L105
Ciotti, L., & Ostriker, J. P. 2001, ApJ, 551, 131
Ciotti, L., & van Albada, T. S. 2001, ApJ, 552, L13
Cole, S., Aragon-Salamanca, A., Frenk, C. S., Navarro, J. F., & Zepf, S. E. 1994, MNRAS, 271, 781
Cole, S., Lacey, C. G., Baugh, C. M., & Frenk, C. S. 2000, MNRAS, 319, 168
Condon, J. J. 1989, ApJ, 338, 13
Connolly, A. J., Szalay, A. S., Dickinson, M., Subbarao, M. U., & Brunner, R. J. 1997, ApJ, 486, L11
Cowie, L L., Songaila, A., Kim T. S., & Hu, E. S. 1995, AJ, 109, 1522
Davé, R., et al. 2001, ApJ, 552, 473
David, L. P., Slyz, A., Jones, C., Forman, W., Vrtilek, S. D., & Arnaud, K. A. 1993, ApJ, 367, 45
Dekel, A., & Silk, J. 1986, ApJ, 303, 39
Di Matteo, T.,Croft, R. A. C., Springel, V., & Hernquist, L. 2003, ApJ, submitted, (astro-ph/0309533)
Efstathiou, G., & Rees, M. J. 1998, MNRAS, 230, 5P
Eisenstein, D. & Hu, W. 1999, ApJ, 511, 5
Eke, V. R., Cole, S., & Frenk C. S. 1996, MNRAS, 282, 263
Ellingson, E., Yee, H. K. C., & Green, R. F. 1991, ApJ, 371, 49
Elvis, M., et al. 1994, ApJS, 95, 1
Fan, X., et al. 2001, ApJ, 121, 54
Ferrarese, L. 2002, ApJ, 578, 90
Fixen, D. J., Cheng, E. S., Gales, J. M., Mather, J. C., Shaver, R. A., & Wright, E. L. 1996, ApJ, 473, 576
Frye, B., Broadhurst, T., & Benitez, N. 2002, ApJ, 568, 558
Fujita, A., Martin, C.L., MacLow, M.-M., & Abel, T. 2003, ApJ, 599, 50
Furlanetto, S. & Loeb, A. 2001, ApJ, 556, 619
Gallego, J., Zamorano, J., Aragón-Salamanca, A., & Rego, M. 1995, ApJ, 455, L1
Glazebrook, K., et al. 2003, in IAU Sump. 216, Maps of the Cosmos, eds. M. Colless & L. Staveley-Smith (San Francisco: ASP)
Granato, G. L., De Zotti, G., Silva, L, Bressan, A., & Danese, L. 2003, ApJ, submitted, (astro-ph/030702)
Grego, L., et al. 2001, ApJ, 552, 2
Haarsma, D. B., Partridge, R. B., Windhorst, R. A., & Richards, E. A. 2000, ApJ, 544, 641
Haehnelt M. G., & Rees M. J. 1993, MNRAS, 263, 168
Haiman Z., & Loeb A. 2001, ApJ, 552, 459
Haiman, Z., Ciotti, L., & Ostriker, J. P. 2003, ApJ, submitted, (astro-ph/0304129)
Hartwick, F. D. A., & Schade, D. 1990, ARA&A, 28, 437
Helsdon, S.F., & Ponman, T.J. 2000, MNRAS, 315, 256
Hernquist, L., & Springel, V. 2003, MNRAS, 341, 1253
Hopkins, A. M., Connolly, A. J., & Szalay, A. S. 2000, AJ, 120, 2843
Hopkins, A. M., Connolly, A. J., Haarsma, D. B., & Cram, L. E. 2001, ApJ, 122, 288

Hu, E. M., et al. 2002, ApJ, 568, L75
Ikeuchi,S. 1981, PASJ, 33, 211
Inoue, S. & Sasaki, S. 2001, ApJ, 562, 618
Kaiser, N. 1986, MNRAS, 222, 323
Kaiser, N. 1991, ApJ, 383, 104
Kauffmann, G., White, S. D. M., & Guiderdoni, B. 1993, MNRAS, 264, 201
Kauffmann, G., Colberg, J. M., Diaferio, A., & White, S. D. M. 1999, MNRAS, 303, 188
Kauffmann G., & Haehnelt M. G. 2000, MNRAS, 311, 576
Kravtsov, A. V., & Yepes, G. 2000, MNRAS, 318, 227
Lacey, C., & Cole, S. 1993, MNRAS, 262, 627
Lewis, G.F., Babul, A., Katz, N., Quinn, T., Hernquist, L., & Weinberg, D. H. 2000, ApJ, 536, 623
Mac-Low, M.-M., & Ferrara, A., 1999, ApJ, 513, 142
Madau, P., Ferguson, H. C, Dickinson, M., Giavalisco, M., Steidel, C. S., & Fruchter, A. 1996, MNRAS, 283, 1388
Madau, P., Pozzetti, L., & Dickinson, M. 1998, ApJ, 498, 106
Majumdar, S., Nath, B., & Chiba, M. 2001, MNRAS, 324, 537
McKee, C. F., & Ostriker, J. P. 1977, ApJ, 218, 148
McLure, R. J., & Dunlop, J. S. 2001, MNRAS, 321, 515
Menci, N., Cavaliere, A., Fontana, A., Giallongo, E., & Poli, F. 2002, ApJ, 575, 17
Menci, N., Cavaliere, A., Fontana, A., Giallongo, E., Poli, F., & Vittorini, V. 2003, ApJ, 587, L63
Merritt, D., & Ferrarese, L. 2001, ApJ, 547, 140
Mo, H. J. & White, S. D. M. 1996, MNRAS, 282, 347
Mo, H. J., Mao, S., & White, S. D. M. 1998, MNRAS, 295, 319
Mo, H. J. & Mao, S. 2002, MNRAS, 333, 768
Monaco P., Salucci P., & Danese L. 2000, MNRAS, 311, 279
Mori, M., Ferrara, A., & Madau, M. 2002, ApJ, 571, 40
Muanwong, O., Thomas, P. A., Kay, S. T., & Pearce, F. R. 2002, MNRAS,336, 527, L5
Natarajan, P., & Sigurdsson, S. 1999, MNRAS, 302, 28
Nath, B., & Silk, J. 2001, MNRAS, 327, L5
Nath, B., & Roychowdhury, S. 2002, MNRAS, 333, 145
Nulsen P. E. J., & Fabian A. C. 2000, MNRAS, 311, 346
Oh, S. P., & Benson, A. 2003, MNRAS, 342, 664
Oh, S. P., Cooray, A., & Kamionkowski, M. 2003, MNRAS, 342, L20
Oh, S. P., & Haiman, Z. 2003, MNRAS, 346, 456
Osterbrock, D. E. 1993, ApJ, 404, 551
Ostriker, J. P., & Thuan, T. X. 1975, ApJ, 202, 353
Ostriker, J. P., & Cowie, L. L. 1981, ApJ, L127
Peebles, P. J. E. 1980, Large Scale Structure of the Universe (Princeton: Princeton University Press)
Pei, Y. C. 1995, ApJ, 438, 623
Pen, U.-L. 1999, ApJ, 510, L1
Perlmutter, S., et al. 1999, ApJ, 517, 565
Pettini, M., Steidel, C. C., Adelberger, K. L., Dickinson, M., & Giavalisco, M. 2001, ApJ, 528, 96
Pierini, D. & Tuffs, R. J. 1999, A&A, 343, 751
Platania, P., Burigana, C., De Zotti, G., Lazzaro, E., & Bersanelli, M. 2002, MNRAS, 337, 242
Porciani, C., Matarrese, S., Lucchin, F., & Catelan, P. 1998, MNRAS, 298, 1097
Pozzetti, et al. 2003, A&A, 402, 837
Pounds, K. A., Reeves, J. N., King, A. R., Page, K. L., O'Brien, P .T., & Turner, M J. L. 2003, MNRAS, 345, 705
Press, W. H., & Schechter, P. 1974, ApJ, 187, 425 (PS)
Proga, D., Stone, J. M., & Kallman, T. R. 2000, ApJ, 543, 686
Rauch, M., Haehnelt, M.G., & Steinmetz, M. 1997, ApJ, 481, 601
Rauch, M., Sargent, W. L., & Barlow, T. A. 2001, ApJ, 554, 823
Rees, M., J., & Ostriker, J. P. 1977, MNRAS, 179, 541
Reese, E. D., Carlstrom, J. E., Joy, M., Mohr, J. J., Grego, L., & Holzapfel, W. 2002, ApJ., 81, 53
Refregier, A., Komatsu, E., Spergel, D.N., & Pen, U.-L. 2000, Phys. Rev. D, 61, 123001
Rowan-Robinson, M., et al. 1997, MNRAS, 289, 490
Scannapieco, E., Ferrara, A., & Broadhurst, T. 2000, ApJ, 536, L11
Scannapieco, E., Ferrara, A., & Madau, P. 2002, ApJ, 574, 590
Scannapieco, E., & Barkana, R. 2002, ApJ, 571, 585
Scannapieco, E., Schneider, R., & Ferrara, A. 2003, ApJ, 589, 35
Scannapieco, E., & Thacker, R. J. 2003, ApJ, 590, L69
Sedov, L. I. 1959, Similarity and Dimensional Methods in Mechanics (New York: Academic)
Serjeant, S., Gruppioni, C., & Oliver, S. 2002, MNRAS, 330, 621
Sheilds, G. A., et al. 2003, ApJ, 583, 124
Shu, F. 1992, The Physics of Astrophysics, Vol II: Gas Dynamics (Universit y Science Books, Mill Valley, California)
Shull, J. M., Tumlinson, J., & Giroux, M.L. 2003, ApJ, 594, 107
Smith, E., Heckman, T., Bothun G., Romanshin, W., & Balick, B. 1986, ApJ, 306, 64
Soltan A., 1982, MNRAS, 200, 115
Somerville, R. S. & Primack, J. S. 1999, MNRAS, 310, 1087
Somerville, R. S., et al. 2003, ApJL, in press (astro-ph/0309067)
Songaila, A. 2001, ApJ, 561, L153
Spergel, D. N., et al. 2003, ApJS, 148, 175
Steidel, C. C., Adelberger, K. L., Giavalisco, M., Dickinson, M., & Pettini, M. 1999, ApJ, 519, 1
Stockton, A., & Ridgway, S. E. 1991, AJ, 102, 488
Strickland, D.K., & Stevens, I.R. 2000, MNRAS, 314, 511
Suginohara, T., & Ostriker, J. P. 1998, ApJ, 507, 16
Sullivan, M., Treyer, M. A., Ellis, R., Bridges, T., Milliard, B., & Donas, J. 2000, MNRAS, 312, 442
Sunyaev, R. A. & Zel'dovich, Ya. B. 1972, Commun. Astrophys. Space Phys., 4, 173
Sutherland, R. S., & Dopita, M. A. 1993, ApJS, 88, 253
Tan, J. C., Silk, J., & Balland, C. 1999, ApJ, 522, 579
Thacker, R. J., Scannapieco, E., & Davis, M. 2002, ApJ, 581, 836
Thomas, D., Greggio, L., & Bender, R. 1999, MNRAS, 281, 323
Tornatore, L, Borgani, S., Springel, V., Matteucci, F., Menci, N., & Murante, G. 2003, MNRAS, 342, 1025
Tozzi, P., & Norman, C. 2001, ApJ, 546, 63
Tozzi, P., Scharf C., & Norman C. 2001, ApJ, 542, 106
Tremaine, S., et al. 2002, ApJ, 574, 740
Tresse, L., & Maddox, S. J. 1998, ApJ, 495, 691
Treyer, M. A., Ellis, R. S., Milliard, B., Donas, J., & Bridges, T. J. 1998, MNRAS, 300, 303
Vader, J. P., Da Costa, G. S., Frogel, J. A., Heisler, C. A., & Simon, M 1987, AJ, 94, 847
van den Bosch, F. C., Abel, T., & Hernquist, L. 2003, MNRAS, 346, 177
Voit, G. M., & Bryan, G. L. 2001, Nature, 414, 425
Voit, G. M., & Ponman T. 2003, ApJ, 594, L75
Warren, S. J., Hewett, P. C., & Osmer, P. S. 1994, ApJ, 42 1, 412
Weymann, R. J., Morris, S. L., Foltz, C. B., & Hewett, P. C. 1991, ApJ, 373, 23
Weymann, R. J. 1997, in Mass Ejection from AGN, eds. N. Arav, I. Shlosman, & R. J. Weymann (San Francsisco: ASP), 3
Willott, C., McLure, R. J., & Jarvis, M. J. 2003, ApJ, 587, 15
Willott, C., Rawlings, S., Blundell, K. M., & Lacy, M. 1999, MNRAS, 309, 1017
Willott, C. J., Rawlings, S., & Greimes, J. A 2003, ApJ, 598, 909
Wyithe, J. S. B., & Loeb, A. 2002, ApJ, 581, 886
Wyithe, J. S. B., & Loeb, A. 2003, ApJ, 595, 614 (WL03)
Wu, K. K. S., Fabian, A. C., & Nulsen P. E. J. 2000, MNRAS, 318, 889
Yamada, M., Sugiyama, N., & Silk, J. 1999, ApJ, 522, 66
Yan, L., McCarthy, P. J., Freudling, W., Teplitz, H. I., Malumuth, E. M., Weymann, R. J., & Malkan, M. A. 1999, ApJ, 519, L47
Yee, H. K. C. & Green, R.. F. 1984, ApJ, 280
Yu, Q. & Lu, Y. 2003, ApJ, in press (astro-ph/0311404)
Yu, Q., & Tremaine, S. 2002, MNRAS, 335, 965

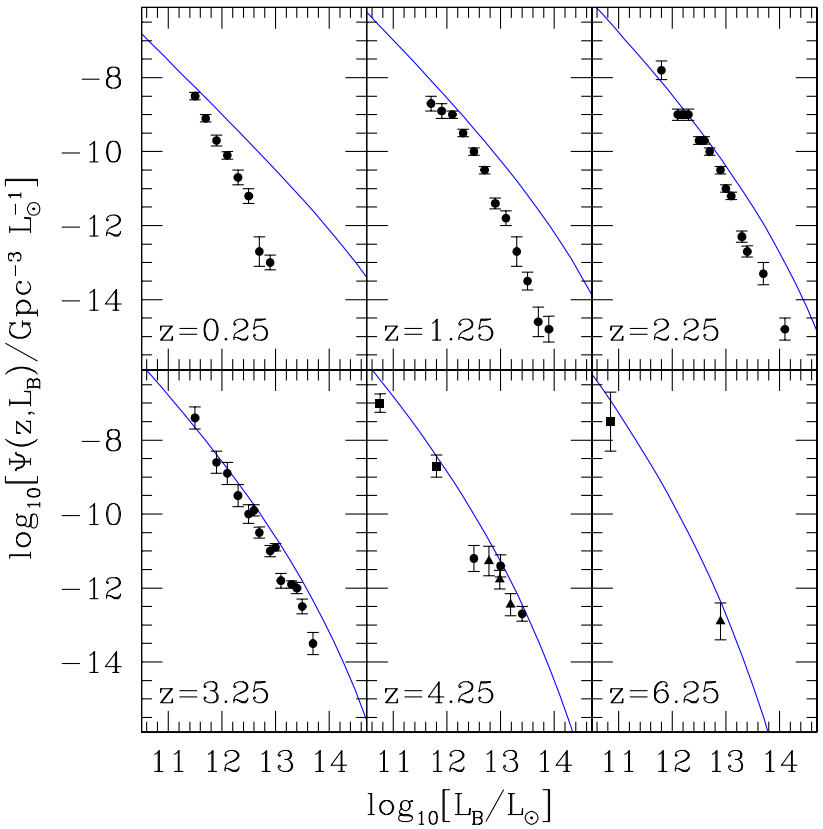


FIG. 1.— Evolution of the B-band quasar luminosity function. Here the data points are taken from Fan (2001, triangles), Pei (1995, circles) as compiled from Hartwick & Schade (1990) and Warren, Hewett, & Osmer (1994), and Barger et al. (2003, squares) as converted from the X-ray in WL03. In all panels the solid lines are the simple WL03 model, with $F = 1.0$.

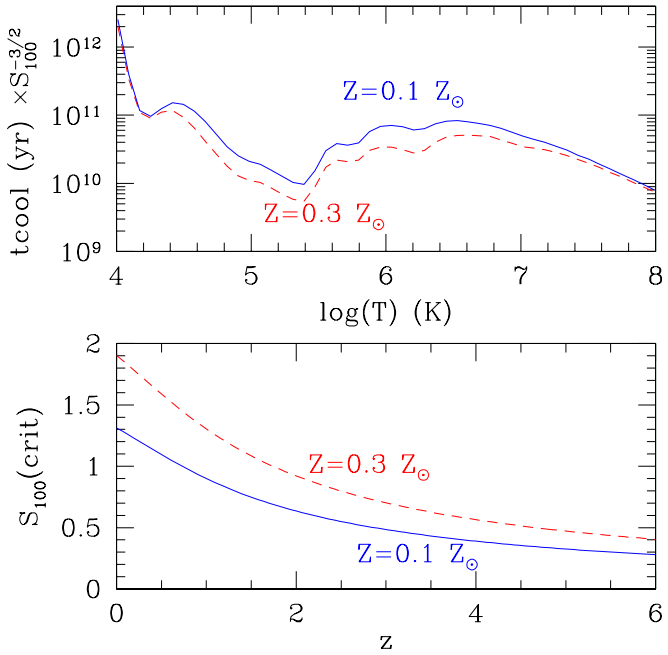


FIG. 2.— *Top:* The cooling time at constant entropy as a function of temperature, for $S_{100} = 1$. Since $t_{\rm cool} \propto S_{100}^{3-2}$, changing S_{100} only shifts the curves up or down the vertical axis. The cooling time has a deep minimum at $T_{\rm min} = 2.3 \times 10^5$K. If the cooling time exceeds the Hubble time at $T_{\rm min}$, it will never be able to cool. *Bottom:* The critical entropy $S_{\rm crit}$ for which $t_{cool}(T_{\rm min}) > t_H$, as a function of redshift.

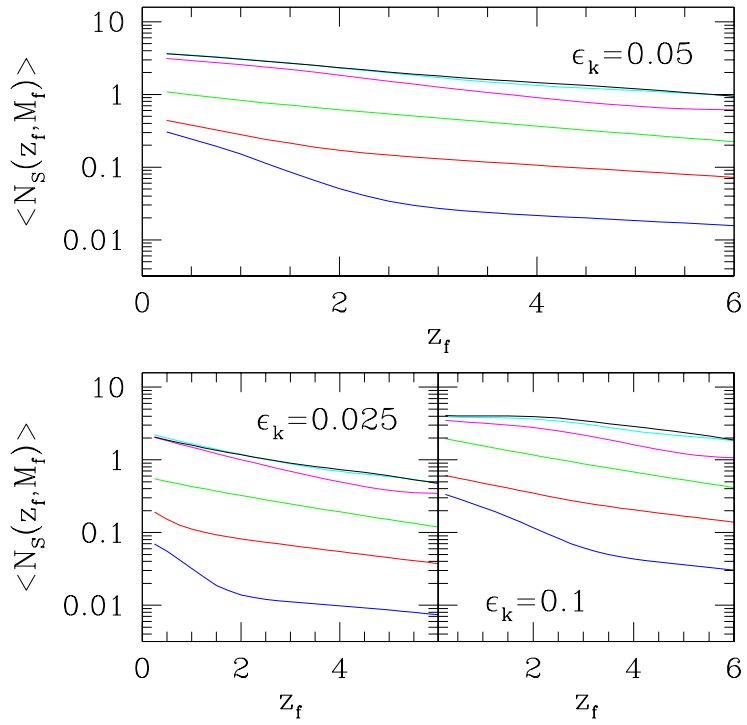


FIG. 3.— Average number of S $S_{\rm crit}$ quasar outflows impacting objects with various formation masses and redshifts. Panels are labeled by their $_k$ values, and in all cases the curves represent masses (from top to bottom) of $10^{15}M$, $10^{14}M$, $10^{13}M$, $10^{12}M$, $10^{11}M$, and $10^{10}M$.

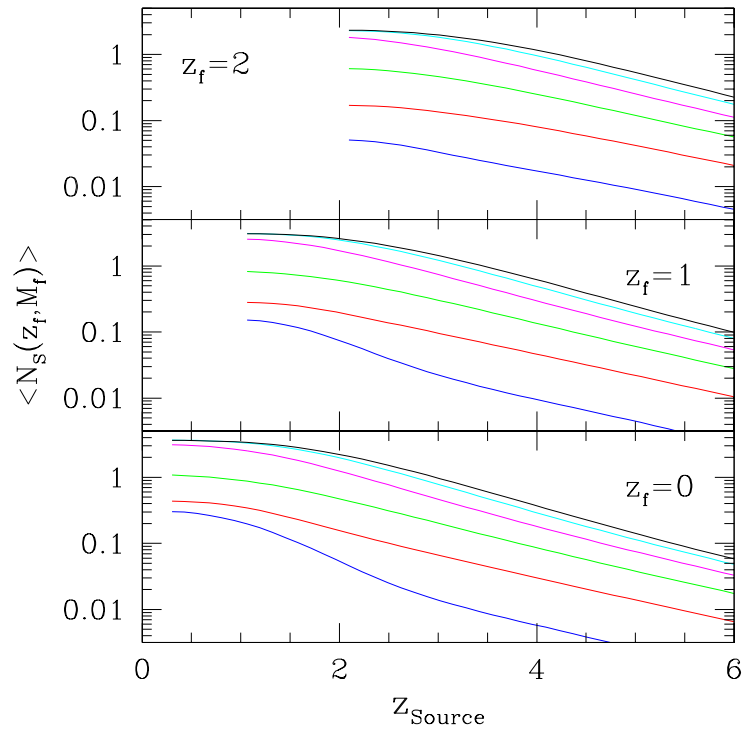


FIG. 4.— Preheating of objects in our fiducial $F = 1$, $_k = 0.05$ model. Here each panel gives the contribution to $N_S(z_f; M_f)$ from sources with redshifts $z_{\rm source}$. Panels are labeled by their z_f values, and in all panels the curves represent masses (from top to bottom) of $10^{15}M$, $10^{14}M$, $10^{13}M$, $10^{12}M$, $10^{11}M$, and $10^{10}M$.

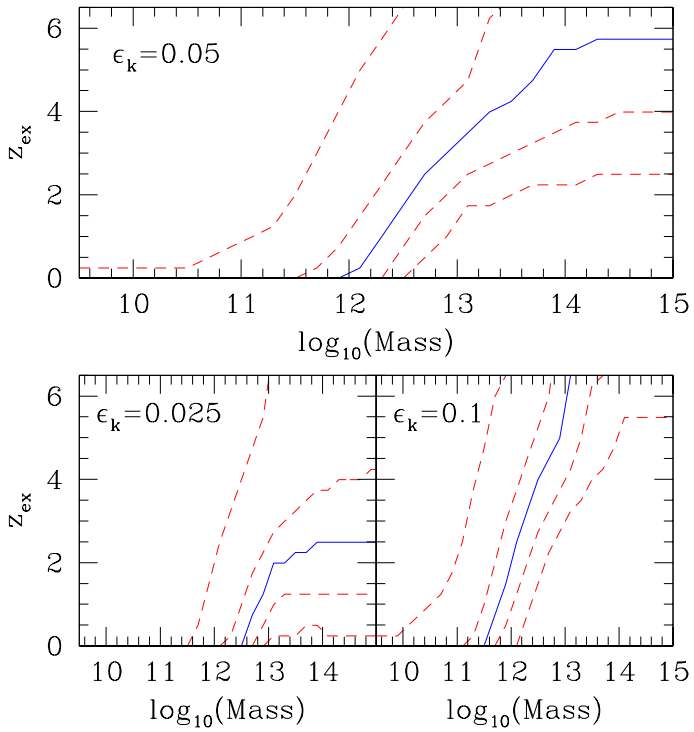


FIG. 5.— "Exclusion redshifts" for various models of quasar heating. In each panel the solid lines show z_{ex} such that $\langle N_S(z_{ex};M)\rangle = 1$; while the short-dashed lines correspond (from top to bottom) to z values such that $f_S(z;M) = 1-\exp\left[-\langle N_S(z;M)\rangle\right]$ = 0.25, 0.5, 0.75, and 0.9. The panels are labeled by their assumed ϵ_k values, and in all cases F = 1.

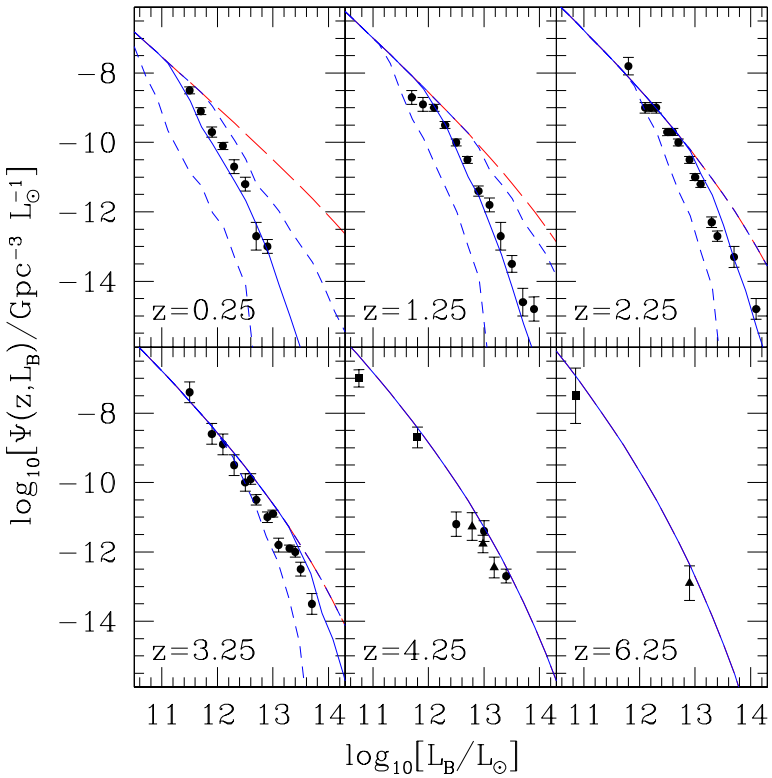


FIG. 6.— Evolution of the B-band quasar luminosity function. In all panels the long-dashed lines are the WL03 model with F = 1.0, the solid lines are our fiducial F = 1.0, ϵ_k = 0.05 model, and the upper and lower short-dashed lines are models in which F = 1.0 and ϵ_k is 0.025 and 0.10 respectively. Points are as in Figure 1.

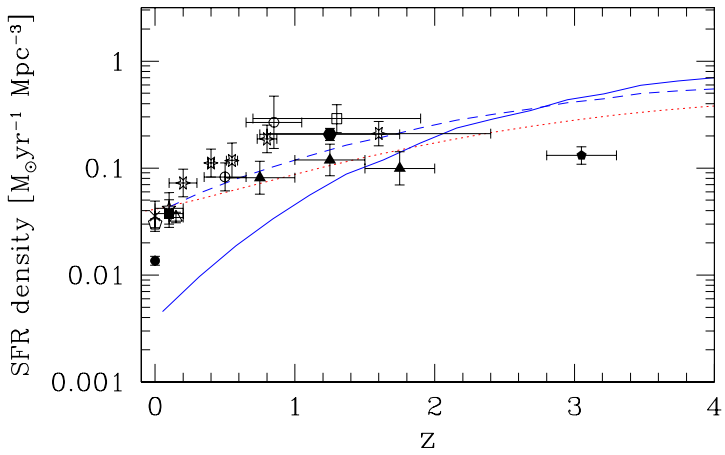


FIG. 7.— Observed and predicted star formation rate densities. Here the solid and short-dashed lines represent the $f_{?} = 0.1$, $f_{?H} = 0.0$ and $f_{?} = 0.05$, $f_{?H} = 0.003$ models, respectively, the dotted line is the fit by Hernquist & Springel (2003), and the points are taken from a wide range of optical, far-infrared, and 1.4 GHz measurements, as compiled and corrected for reddening by Hopkins et al. (2001), and converted to our assumed cosmology. In particular, the symbols represent measurements by Haarsma et al. (2000) (six-pointed stars), Hopkins, Conolly, & Szalay (2000) (solid hexagons), Sullivan et al. (2000) (five-pointed stars), Serjeant et al. (2002) (open pentagons), Steidel et al. (1999) (filled pentagons), Yan et al. (1999) (open squares), Treyer et al. (1998) (filled squares), Tresse & Maddox (1998) (open triangles), Connolly et al. (1997) (filled triangles), Rowan-Robinson et al. (1997) (open circles), Gallego et al. (1995) (filled circles), and Condon (1989) (crosses).

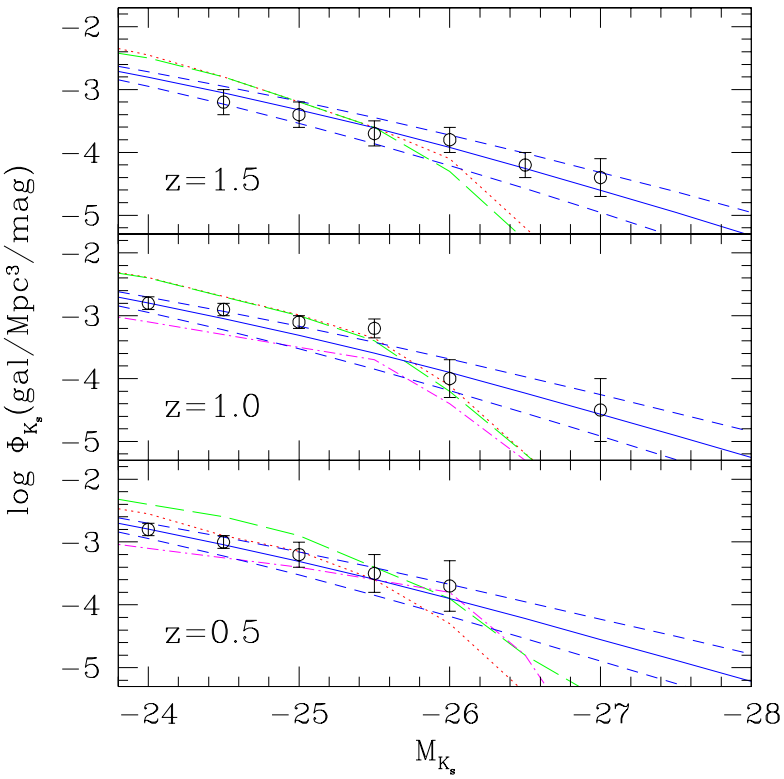


FIG. 8.— The rest-frame K_s band luminosity function of luminous galaxies. In each panel the solid lines represent our fiducial $F = 1$, $_{k} = 0.05$ model, while the $_{k} = 0.025$ and $_{k} = 0.10$ models are given by the upper and lower short-dashed lines respectively. The points are the K_s band observations from Pozzetti et al. (2003), and the dotted, long-dashed, and dot-dashed lines represent the Menci et al. (2002), Cole et al. (2000), and Kauffmann et al. (1999) models, respectively, as compiled by Pozzetti et al. (2003). Quasar feedback naturally turns off massive galaxy formation at low redshifts, reproducing the observed lack off evolution in the number density of luminous galaxies below z 1.5.

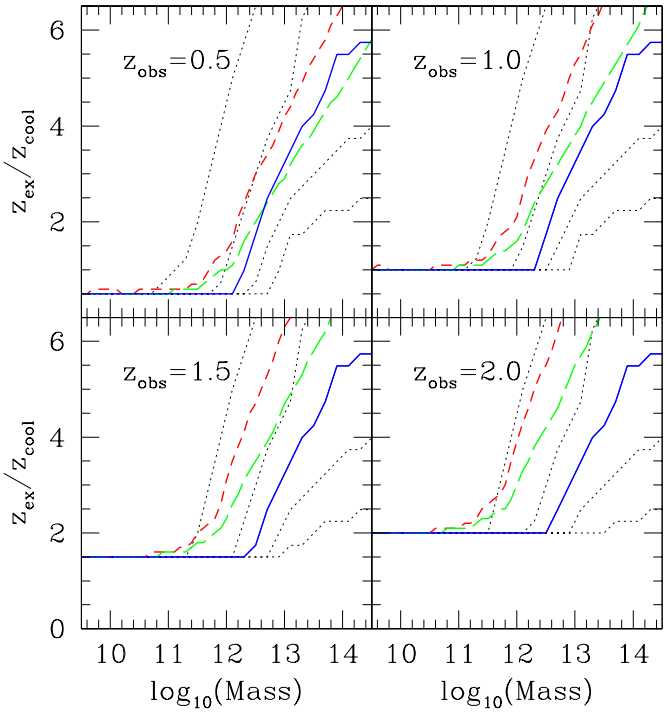


FIG. 9.— Comparison between galaxy regulation by post-virialization cooling and quasar feedback. In each panel the solid line shows the last redshift of formation as defined by z_{ex} in our fiducial model, while the short-dashed and long-dashed lines impose post-virialization criteria according to eq. (42), with $f = 1$ and $f = 1=2$; respectively. Finally the dotted lines correspond (from top to bottom) to z values such that $f_S(z;M) = 0.25$, 0.5, 0.75, and 0.9, as in Figure 5.

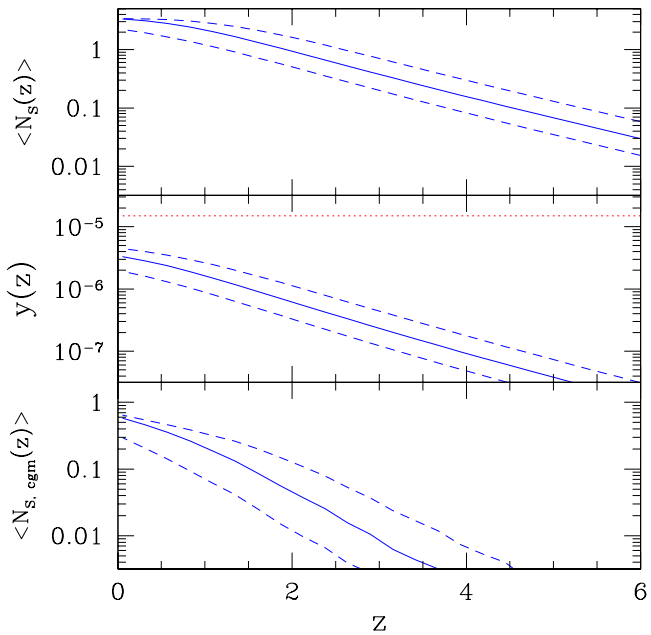


FIG. 10.— Global impact of quasar outflows on the intergalactic medium. *Top:* The mean number of $S \quad S_{crit}$ outflows impacting a random point in space as computed from eq. (20). Here the solid line is given by our fiducial $_k = 0:05$ model, while the upper and lower dashed lines correspond to the $_k = 0:10$ and $_k = 0:025$ models respectively. *Center:* Compton-y parameter as computed from eq. (43). Solid and dashed lines are as in the top panel, while the dotted line is the observational limit of $y \quad 1:5 \quad 10^{-5}$ (Fixen et al. 1996). *Bottom:* Mass fraction of heated gas in a typical region of circumgalactic gas, associated with the Ly forest at $z > 2$ and the WHIM at low redshifts, as computed from eq. (45). Lines are as in the top panel.

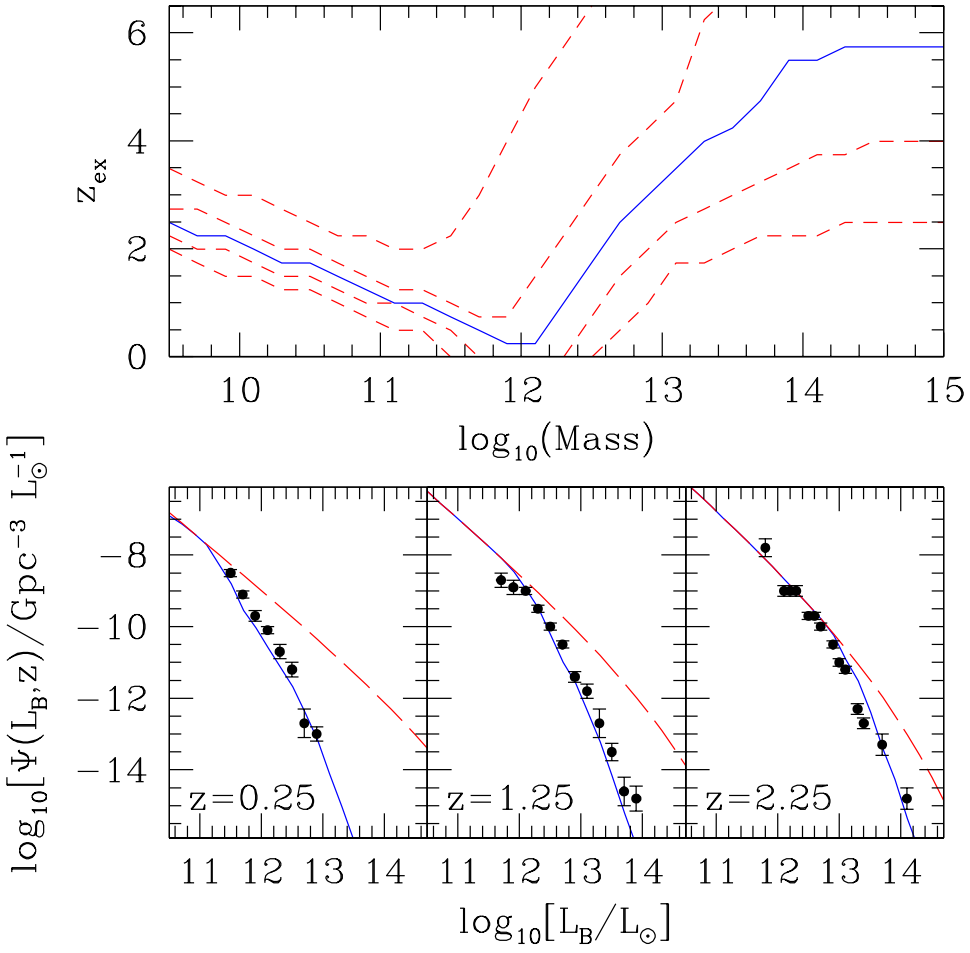


FIG. 11.— Comparison between feedback through $S < S_{\rm crit}$ heating and the baryonic stripping of objects, which dominates in high-redshift starbursts. *Top:* As in Figure 5, the solid line shows $z_{\rm ex}$ such that $\langle N_S(z_{\rm ex};M)\rangle = 1$; while the short-dashed lines correspond (from top to bottom) to z values such that $f_S(z;M) = 1-\exp\left[-\langle N_S(z;M)\rangle\right] = 0.25$, 0.5, 0.75, and 0.9. While quasars are able to strip the gas out of small perturbations that are not heated above $S_{\rm crit}$; this occurs relatively late, long after the majority of objects in this mass range have formed. *Bottom:* Quasar luminosity function. In all panels the solid line is our fiducial model, but including the additional feedback from baryonic stripping, while the long-dashed lines are the WL03 model. Points are in Figure 1. Stripping occurs too late to have any impact on these results.